NORMALIZING ABERRANT VASCULATURE CHARACTERISTICS GENERATED BY ELEVATED EXTRACELLULAR MATRIX STIFFNESS

A Thesis

Presented to the Faculty of the Graduate School

of Cornell University

In Partial Fulfillment of the Requirements for the Degree of

Masters of Science

by

Emmanuel Macklin Lollis

January 2017

ABSTRACT

Tumor blood vasculature tends to be heterogeneously distributed, densely branched, tortuous, malformed, and hyperpermeable relative to that found within physiological tissues. Furthermore, tumors are known to stiffen as they progress, a phenomenon that has largely been attributed to heightened extracellular matrix protein cross-linking. As cells are capable of sensing and responding to the stiffness of their surrounding matrix via mechanisms that include changes in the phosphorylation of focal adhesion proteins, like FAK and Src, we hypothesized that there is a relationship between abnormal tumor vasculature characteristics and tumor stiffening. By grafting glycated collagen constructs to the chorioallantoic membranes of chicken embryos cultured ex ovo, and with two- and three-dimensional human umbilical vein endothelial cell culture systems, we show that increasing the stiffness of a tissue significantly enhances the extent of angiogenic vascularization it experiences, and that neovessels or monolayers formed within stiff tissues or on stiff substrates are significantly more permeable than their compliant counterparts. Furthermore, we demonstrated that membrane type-one matrix metalloproteinase activity inhibition can nullify the effect that matrix stiffening has on vascularization ex ovo, and that inhibiting the phosphorylation of FAK tyrosine residue 397 (Y397) can alleviate stiffness-induced hyperpermeability in vitro and ex ovo. Using western blotting techniques, we show that Src Y418 and VE-cadherin Y685 phosphorylation significantly increase with increasing matrix stiffness, and that FAK inhibition prevents the latter from occurring. Together, these data indicate that matrix stiffening promotes the phosphorylation of Src, and that Src interacts with activated FAK to phosphorylate tyrosine residues on the cytoplasmic tail of VE-cadherin, which regulate endothelial barrier junction integrity via the mediation of catenin attachment. We conclude by suggesting co-treatments to enhance the efficacy of existing chemotherapeutics, and by conceptualizing future projects that expand upon the work presented here.

BIOGRAPHICAL SKETCH

Emmanuel Macklin Lollis was born and raised in Buffalo, New York. In 2014, he graduated *summa cum laude* from University at Buffalo with a Bachelor's of Science degree in Chemical and Biological Engineering. During his time as an undergraduate student, Emmanuel proudly worked at Wegmans Food Markets for four years, volunteered at the Buffalo VA Medical Center, joined the ranks of Tau Beta Pi, and investigated an exogenous protein therapy capable of alleviating the cytotoxicity of chemotherapeutics and of enhancing the proliferative capacity of cardiomyocytes within the Tzanakakis lab, which yielded him a Senior Scholar Award from the School of Engineering and Applied Sciences. Furthermore, Emmanuel became a two-time recipient of the UB CBE Academic Excellence Award, and of the very generous Wegmans Scholarship Program. Following that, he pursued graduate study at Cornell University.

As a member of the School of Chemical and Biomolecular Engineering, Emmanuel joined the Reinhart-King lab to study the effect that extracellular matrix stiffness has on tissue vascularization, with a focus on cancer applications. During his time as a graduate student, Emmanuel served as a teaching assistant to *Introduction to Chemical Engineering*, and to *Biomaterials: Foundations and Applications in Medicine*. In addition to performing required duties, he took the opportunity to generate novel problems, and to design and instruct lectures. In recognition of his passion for teaching, Emmanuel was selected to become a fellow of the Graduate Assistantships in Areas of National Need Fellow program. In addition to research, teaching, and coursework, Emmanuel also designed, led, and participated in numerous outreach programs. Following the presentation of this thesis, he will proudly graduate from Cornell University with a Master's of Science degree in Chemical and Biomolecular Engineering.

ACKNOWLEDGEMENTS

I would like to begin by expressing my sincerest and deepest gratitude toward Professor Cynthia A. Reinhart-King, who recruited me to join her lab despite unusual circumstances, mentored me in both my research and personal development with patience and understanding, helped me identify and procure the funding that facilitated my graduate studies, supported my passion for teaching, and inspired me to fight for my education while going out of her way to ensure that I had a positive experience at Cornell University. Were it not for your continued support and guidance, I would not have made it as far as I have. I will always appreciate your generosity and consideration, and I aspire to make you proud in my future endeavors.

I would also like to thank numerous members of the Reinhart-King lab, including: Michael C. Mazzola, who shared his knowledge regarding *ex ovo* chicken embryo culture with me prior to graduating, and thus helped me achieve a running start in my research; Danielle J. LaValley, who taught me nearly all of the *in vitro* methods that I utilized in this project, and who helped me troubleshoot a handful of experiments; Dr. François Bordeleau, who consulted me on experimental design, helped me troubleshoot numerous experiments, and who placed trust in me by allowing me to help him with his own experiments; Julie C. Kohn and Joseph P. Miller, who encouraged me to become a more outgoing individual; Lauren A. Hapach, who synthesized most of the collagen used in my experiments; and the many others who made my time within the Reinhart-King lab a pleasure.

Furthermore, I would like to thank Professor Susan Daniel, who oversaw my progression as a graduate student in her capacity as the Director of Graduate Studies within the School of Chemical and Biomolecular Engineering, and as a member of my special committee, and Professor Abraham D. Stroock, who also oversaw my progression as a graduate student in his capacity as Director of the School of Chemical and Biomolecular Engineering, as instructor to *Advanced Principles of Biomolecular Engineering*, and as a member of my special committee.

I would also like to thank Professor Rebecca M. Williams and Dr. Johanna M. Dela Cruz of the Cornell University Biotechnology Resource Center Imaging Facility, who trained me on equipment that was vital to my success. Furthermore, I would like to thank Professor Jonathan T. Butcher for allowing me to use equipment within his lab to conduct chicken embryo culture.

For helping me in a difficult time, I would like to extend a big thanks to Jason Kahabka and Janna S. Lamey, who ensured that I had a successful experience at Cornell University.

I would like to thank Professor Christopher A. Alabi, who I worked under in my capacity as head teaching assistant to *Introduction to Chemical Engineering*. His friendly demeanor, enthusiasm, and willingness to share creative control over the course fueled my passion for teaching. Of all my time at Cornell University, the semester that I spent as a teaching assistant under Professor Alabi was the most enjoyable. Furthermore, I would like to thank Professor Schivaun D. Archer and Professor Chris B. Schaffer, who selected me to become a recipient of the Graduate Assistantships in Areas of National Need fellowship program, and Dr. Shalu Suri, who I worked with in my capacity as a GAANN fellow and as a teaching assistant to help instruct *Biomaterials: Foundations and Applications in Medicine.*

I would also like to thank Professor Emmanuel S. Tzanakakis, who recruited me to perform undergraduate research within his lab, and Dr. Ivanna Ihnatovych, who selflessly taught me numerous techniques, trusted me with her own experiments, and supervised my work. On that note, I would also like to thank a number of my undergraduate professors, including Professor Chong Cheng, Professor Johannes M. Nitsche, Professor Tamara G. Kofke, Professor Marina Tsianou, Professor Carl R. F. Lund, Professor Jeffrey R. Errington, Professor Blaine Pfeifer, Professor Edward P. Furlani, Professor Michael J. Lockett, and Professor Mark T. Swihart.

I would like to thank Dr. Andrew J. Greenshields, who encouraged me to pursue a challenging education, and who introduced me to the field of chemical engineering. I will always be grateful to you, as your insight and wise advice placed me on my current trajectory.

I would also like to thank my former manager and co-workers within the deli at the Wegmans on Niagara Falls Boulevard, who became as close as family to me during the four years that I worked with them. Some of my warmest memories are of the times that I spent with you, and I am fortunate to have been exposed to your strong, thorough, positive work ethics.

Finally, I would like to thank my close friends and family. Without your continuous love, support, and encouragement, I would never have made it to where I am today.

TABLE OF CONTENTS

LIST OF FIGURES

LIST OF ABBREVIATIONS

1°abs or 2°abs	Primary or Secondary Antibodies
2D or 3D	Two- or Three- Dimensional
AA	Acetic Acid
AGE	Advanced Glycation End Product
APS	Ammonium Persulfate
BAEC	Bovine Aortic EC
BAPN	β-aminopropionitrile
bFGF	Basic FGF
BSA	Bovine Serum Albumin
CAM	Chorioallantoic Membrane
DMSO	Dimethyl Sulfoxide
ECM	Extracellular Matrix
EC	Endothelial Cell
ED	Embryonic Day
EGM	Endothelial Growth Media
EtOH	Ethanol
Ex-Ovo	Outside of the Egg
FAK	Focal Adhesion Kinase
FGF	Fibroblast Growth Factor
FITC	Fluorescein Isothiocyanate
GAPDH	Glyceraldehyde 3-Phosphate Dehydrogenase
GM6001	A Small-Molecule Inhibitor of MMP Activity

HEPES	4-(2-hydroxyethyl)-1-piperazineethanesulfonic acid
HIF	Hypoxia Inducible Factor
HUVEC	Human Umbilical Vein Endothelial Cells
In-Vitro	Outside of a Living Organism
In-Vivo	Within a Living Organism
IR	Intensity Ratio
LOX and LOXL2	Lysyl Oxidase and Lysyl Oxidase-Like 2
LSM	Laser Scanning Microscopy
MPM	Multi-Photon Microscopy
MT1-MMP or MMP14	Membrane-Type I Matrix Metalloproteinase
MQ	*Milli*-Q
N6	N-6-((acryloyl)amido) Hexanoic Acid
NIR	Normalized Intensity Ratio
P3 or P7	Cell Passage 3 or 7
PA	Polyacrylamide
PBS	Phosphate-Buffered Saline
PF573228	A small-molecule inhibitor of FAK Y397 phosphorylation
PGDF	Platelet-Derived Growth Factor
PVDF	Polyvinylidene Difluoride
ROI	Region of Interest
RTT	Rat Tail Tendon
SDS	Sodium Dodecyl Sulfate
SMC	Smooth Muscle Cell

Src	Proto-Oncogene Tyrosine-Protein Kinase
TBS or TBS-t	Tris-Buffered Saline, or Tris-Buffered Saline with Polysorbate 20
TEMED	Tetramethylethylenediamine
TM	Tetrathiomolybdate
Tris	2-Amino-2-(hydroxymethyl)propane-1,3-diol
TRITC	Tetramethylrhodamine
VE-cadherin	Vascular Endothelial Cadherin
VEGF	Vascular Endothelial Growth Factor
Y397, Y418, Y658, or Y685	Tyrosine Residue 397, 418, 658, or 685

CHAPTER 1

INTRODUCTION

1.1 Abnormal Tumor Vasculature

The American Cancer Society estimates that nearly six-hundred thousand Americans will succumb to cancer in 2016, making it the second leading cause of death within the United States.[1] Cancer is characterized by the dysregulated growth of malignant neoplasms, or tumor-forming masses of invasive cells. If limited to known, accessible regions of the body, cancerous tissue can be excised. However, the majority (≥90%) of cancer-related deaths are attributed to complications caused by secondary tumors, which arise from metastasis.[2,3] Therefore, most existing cancer treatment methods, including chemotherapy and immunotherapy, hormone therapy, and targeted therapy, rely heavily on the use of systemic agents to combat malignant cells.[4,5] These are often administered alongside radiotherapy, the efficacy of which is a function of cell oxygenation, and photodynamic therapy, which utilizes systemic photosensitizers.[4–6] Within tumors, vasculature with abnormal characteristics generates physical and biochemical conditions that resist the entry of systemic agents, drive metastasis, and alter cell phenotypes.[7,8]

Tumor blood vasculature tends to be heterogeneously distributed, densely branched, tortuous, malformed, and hyperpermeable relative to that found within physiological tissues.[9,10] Due to a large number of leaky vessels, the interstitial space fills with fluid. Without functional lymphatic vessels to drain this fluid, and in conjunction with tumor cell proliferation and elevated extracellular matrix (ECM) protein deposition, interstitial pressures surpass venous pressures, leading to vessel collapse and flow stasis or reversal.[9,11] This exasperates flow rate issues precipitated by excessive branching, tortuosity, malformations, and elevated intratumoral blood viscosities.[9–12] As a result, convective flow through and extravasation into tumors, the primary driving forces behind drug transport, are largely absent. In fact, as interstitial pressure drops to normal levels at the periphery, flow tends to evade tumors, as evident by their hypoxic,

acidic cores.[7,9] This limits intratumoral drug transport to diffusion, which faces an excessive collagen-rich extracellular matrix, and which must reach regions that lack vasculature.[7] Thus, systemic drugs can pass through the body without ever penetrating the tumor.[7,13] Equivalently, the entry of lymphocytes responsible for eliminating dysfunctional cells is also hindered, and the function of those that do enter are impaired by hypoxic and acidic conditions.[14] In contrast, outward flow through compromised vessels facilitates the escape of metastatic cells, and a hypoxic environment promotes invasive phenotypes.[14]

Angiogenesis, the physiological process by which new vascular networks sprout from existing ones, is a process mediated by numerous pro- and anti- angiogenic factors.[15] In the early 1970s, Judah Folkman identified that solid tumor growth beyond a few millimeters, the size above which the diffusion of nutrients and oxygen becomes inadequate, requires the presence of local vasculature, and thus is the limiting factor in tumor growth.[16] Based on this observation, he hypothesized that suspending tumors in a nonvascularized state via anti-angiogenic therapy would isolate metastasizing cells from the rest of the body, enhance the efficacy of chemotherapeutics, and facilitate immunologic attacks.[17] However, it has since been shown that disrupting tumor vasculature has the opposite effect: it introduces hypoxia, which fuels tumor growth and aggression, it removes the infrastructure that systemic agents rely on to infiltrate tissue, and it generates a microenvironment that impairs immune cell entry and function.[14] The field now believes that the meager improvements observed in the prognosis of patients receiving anti-angiogenic therapy may be attributed to brief periods of vascular normalization.[14,18]

1.2 Tumor Stiffening

In addition to possessing abnormal vasculature, tumors also stiffen as they progress; the elastic moduli of some tumors rise to manyfold that of healthy tissue.[19] This stiffening has been attributed to increased extracellular matrix protein deposition, cell crowding, fluid accumulation,

matrix remodeling, and elevated ECM protein cross-linking.[20] Of these, the cross-linking of ECM proteins, namely collagen, is believed to drive matrix stiffening.[21]

In healthy tissues, collagen, the most abundant protein in the human body, forms networks of fibers that provide tissue with its tensile strength.[22] As tissues age, the aldehyde groups of reducing sugars, like glucose and ribose, react non-enzymatically with the free amino groups of lysine and arginine residues of collagen to form Schiff bases, which can spontaneously rearrange into Amadori products, which can undergo further reactions to form a variety of advanced glycation end-products (AGEs), which can form intramolecular covalent cross-links with other AGE-containing proteins.[23] Owing to the hypoxic nature of tumor tissue, which restricts the cells within them from performing aerobic respiration, tumors uptake and process glucose at a higher rate than normal tissues via anaerobic glycolysis, suggesting an increase in AGE formation.[24] Collagen fibers can also be enzymatically cross-linked via lysyl oxidase (LOX), which oxidizes collagen lysine and arginine residues to α-aminoadipic-δ-semialdehydes, which spontaneously condense to form intramolecular covalent cross-links with similarly affected fibers.[25] Increases in LOX expression and secretion have been linked to hypoxia, and is largely regarded as the driving force responsible for tumor stiffening and progression.[21,26–28]

Over the past two decades, significant evidence indicating that cells are capable of sensing and responding to the mechanical properties of their surrounding extracellular matrix has emerged.[29,30] Notably, changes in ECM stiffness can influence cell differentiation, gene and protein expression, proliferation, survival, spreading, polarization, adhesion, migration, and cell-cell interactions.[31] Cells adhere to and sense surrounding matrix proteins via integrin receptors, which cluster and link to the actin cytoskeleton through multi-protein focal adhesion complexes.[30] In addition to providing scaffolding functions, many of these proteins participate in numerous signaling pathways. Of these, focal adhesion kinase (FAK) and proto-oncogene tyrosine-protein kinase (Src) have been implicated in stiffness-sensing mechanisms.[32,33]

1.3 Relationship Between Tumor Stiffening and Abnormal Tumor Vasculature

The aberration of tumor vascular characteristics is commonly attributed to an increased presence of pro-angiogenic factors, including, but not limited to, vascular endothelial growth factors (VEGFs), fibroblast growth factors (FGFs), hypoxia-inducible factors (HIFs), platelet-derived growth factors (PDGFs), and angiopoietins.[34] Therefore, vascular normalization experts advocate the judicious administration of anti-angiogenic agents, hypothesizing that doing so will counteract the excessive angiogenic stimuli that upset the balance of the process, which ultimately leads to the formation of abnormal vasculature.[35] These attempts have met with limited success, typically only extending patient life by weeks to months when used in conjunction with existing chemotherapeutics.[8,14] However, angiogenesis is a product of multiple stiffness-dependent cell processes, including proliferation, differentiation, polarization, adhesion, and migration.[15,36,37] Therefore, it, too, is likely influenced by tissue stiffness.

Recent efforts to investigate the effect that tissue stiffness has on angiogenesis in the context of tumor stiffening have largely relied upon the manipulation of construct density and composition.[38–40] These studies reported decreases in angiogenic outgrowth and vascular network formation with increasing tissue stiffness. However, as ECM protein density is inherently linked to matrix architecture, porosity, and the number of available integrin binding sites, all of which influence cell functions involved in angiogenesis, the influence that matrix stiffness has on angiogenesis could not be singled out.[41] Furthermore, recent work published by our lab revealed that bovine aortic endothelial cells (BAECs) embedded in cross-linked collagen gels exhibit enhanced angiogenic outgrowth relative to those embedded in compliant gels.[41] Therefore, this project begins with an investigation into the effect that collagen fiber cross-linking has on angiogenic vascularization. Furthermore, as matrix stiffness has been shown to influence the activity of membrane-type 1 matrix metalloproteinase (MT1-MMP, or MMP14), a mediator of angiogenesis, its role on stiffness-dependent vascularization was determined.[42–44]

In the context of arteriosclerosis, prior work published by our lab suggested that stiffening of the arterial intima, which occurs naturally with age, leads to increases in vascular permeability.[45] This was achieved by seeding BAECs on synthetic two-dimensional (2D) polyacrylamide gels functionalized with collagen, and by means of an Evan's blue permeability assay in young and old mice. The intima consists of a one-cell-thick lining of endothelial cells surrounded by a thin basement membrane, which, in large vessels, is composed of collagen, elastin, and proteoglycans.[46,47] While the intima of arteries and veins are surrounded by a media composed mainly of smooth muscle cells (SMCs), and by an adventitia composed of connective tissue, that of angiogenic neovessels and tumor microvessels only receives partial shelter from pericytes.[48,49] Therefore, not only is the extracellular component of their intima exposed to the same cross-linking reactions taking place within the tumor stroma, but the endothelial lining within it has little cushion from the forces imposed by the surrounding tumor matrix. That motivation established, this project proceeds with an investigation into the effect that matrix stiffness, independent of matrix density, has on the permeability of tumor vessels.

1.4 Potential Targets in Normalizing Stiffness-Dependent Vascular Permeability

Outside of the blood-brain barrier, endothelial cells within blood vessels adhere to one another and regulate permeability via adherens junctions, which are maintained by vascular endothelial (VE)-cadherin.[50] Since our lab has previously shown that increasing matrix stiffness disrupts endothelial barrier junction integrity, we sought to uncover the mechanism responsible for stiffness-induced permeability.[45] Furthermore, it has been well established that the phosphorylation of VE-cadherin's cytoplasmic tail mediates vascular permeability. Tyrosine residue 658 (Y658) phosphorylation disrupts the binding of the junction stabilizer proteins p120-catenin and β-catenin, resulting in junction disassembly and a decrease in endothelial barrier function.[51–55] Phosphorylation of a separate tyrosine residue, Y685, has also been found to trigger vascular permeability.[51,52,56] Relevantly, phosphorylation of FAK Y397 and Src Y418 have been shown to directly phosphorylate VE-cadherin residues Y658 and Y685.[33,56–58]

Increases in the expression and activity of FAK and Src, two cytoplasmic protein tyrosine kinases that associate with focal adhesions and participate in numerous signaling pathways, has been correlated to poor prognosis in cancer patients.[59–62] Phosphorylation of FAK Y397, which has been reported to increase with matrix stiffness, as well as in response to integrin engagement, recruits Src to focal adhesions, where both undergo additional phosphorylation events.[59–62] In multiple studies, FAK and Src have been reported as mediators of vascular permeability.[63–67] Because FAK Y397 itself has been implicated in influencing vascular permeability, and because it recruits and activates Src, as well as forms FAK-Src complexes that trigger additional phosphorylation events, we chose to investigate the ability of PF573228, an inhibitor of FAK Y397 phosphorylation, to restore the integrity of leaky neovessels.[61,62,68–71]

1.5 Project Overview

Based on what is known about tumor stiffening and abnormal tumor vasculature, we hypothesized that angiogenesis is mediated by extracellular matrix stiffness, and that the extent to which a tissue experiences angiogenic vascularization is a function of its stiffness. To investigate the effect that matrix stiffness has on angiogenic vascularization, constructs containing collagen gels of various stiffness were grafted to the chorioallantoic membranes (CAMs) of chicken embryos cultured *ex ovo* on day 10 of embryonic development (ED10). Collagen stiffness was mediated by initiating non-enzymatic glycation reactions with ribose prior to gel polymerization, which produced three-fold increases in gel equilibrium compressive modulus without producing significant changes in fiber architecture.[72] These glycated collagen gels were infused with VEGF and basic FGF (bFGF) to induce angiogenesis, and constructs were formed by sandwiching the gel between nylon meshes to separate the gel from existing vasculature, as well as to provide a grid for quantification.[73] On ED13, neovessels were counted with the aid of a stereoscope, and vascular density was defined as the percentage of squares within the grid containing vasculature. From these experiments, we found that stiffer constructs contained significantly denser vascular networks than their compliant counterparts. To

investigate the role that MT1-MMP activity plays in stiffness-dependent vascularization, GM6001, an inhibitor of MMP activity, was introduced to select constructs. Interestingly, we found that while MMP inhibition has no effect on the vascularization of compliant constructs, it reduces the vascularization of stiff constructs to compliant construct levels.

Furthermore, we hypothesized that angiogenic neovessel and tumor blood microvessel endothelial barrier integrity is a function of extracellular matrix stiffness, and that vascular permeability increases with increasing matrix stiffness. To investigate the effect that matrix stiffness has on endothelial barrier integrity, an *in vitro* monolayer permeability assay was conducted on human umbilical vein endothelial cell (HUVEC) monolayers grown on compliant and stiff collagen-functionalized polyacrylamide (PA) gel substrates. To quantify monolayer permeability, endothelial cell (EC) monolayers were introduced to media containing 40 kDa fluorescein isothiocyanate (FITC)-dextran, and confocal laser scanning microscopy (LSM) was used to capture the fluorescent signal intensity above and below the monolayer after a set time. Following analysis, we found that increasing substrate stiffness yields significantly leaker HUVEC monolayers. To further investigate the effect that matrix stiffness has on vascular permeability, we developed a novel assay to quantify the permeability of chicken embryo CAM angiogenic neovessels grown within grafted collagen constructs. This was achieved by injecting fifteen day old chicken embryos with a mixture of 2 MDa FITC-dextran and 65-85 kDa tetramethylrhodamine (TRITC)-dextran, and multi-photon microscopy (MPM) was used to identify neovessels and to record fluorescent dye extravasation over time. Following analysis, we found that stiffer constructs contained significantly leakier neovessels than their compliant counterparts. To substantiate the validity of our model, positive control samples were generated by introducing VEGF, which is known to induce hyperpermeability, to the injection mixture.[74] We found that, regardless of construct stiffness, the neovessels of chicken embryos injected with VEGF became significantly more leaky.

Motivated by findings that matrix stiffness can disrupt vascular permeability, we decided to investigate the ability of PF573228, an inhibitor of FAK Y397 phosphorylation, to restore the integrity of leaky endothelial barriers in contact with stiff matrices. By running *in vitro* monolayer permeability assays on HUVEC monolayers grown on collagen-functionalized PA gels, we found that treatment with PF573228 significantly reduces the permeability of monolayers grown on stiff substrates, but does not influence that of those grown on compliant ones. Inspired by these findings, we applied PF573228 to collagen constructs grafted to the CAMs of chicken embryos cultured *ex ovo*, and quantified the effect that FAK inhibition has on neovessel permeability. Surprisingly, we found PF573228 capable of reducing the permeability of neovessels within stiff constructs to compliant construct levels.

Finally, we decided to investigate the mechanism responsible stiffness-sensitive vascular permeability. To accomplish this, western blotting techniques were applied to compliant and stiff HUVEC-infused glycated collagen gels, some treated with PF573228. Because we hypothesized that stiffness-induced hyperpermeability is elicited by the phosphorylation of VE-cadherin's cytoplasmic tail, which FAK and Src activity are known to mediate, we decided to probe FAK, Src, and VE-cadherin phosphorylation as a function of matrix stiffness and FAK inhibition. We verified that PF573228 inhibits FAK Y397 phosphorylation, as intended. Furthermore, we found that Src Y418 and VE-cadherin Y685 phosphorylation significantly increase with increasing matrix stiffness, and that FAK inhibition prevents the latter from occurring.

Additional experiments were conducted over the course of this project, including an investigation into the effect that collagen cross-linking via glutaraldehyde has on angiogenic outgrowth *ex ovo*, the effect that β-aminopropionitrile (BAPN) has on EC monolayer permeability *in vitro*, and the effect that matrix stiffness via collagen cross-linking has on MT1-MMP expression and activity in ECs cultured within glycated collagen gels.

CHAPTER 2

MATERIALS AND METHODS

2.1 *In Vitro Techniques*

2.1.1 Cell Culture

Human umbilical vein endothelial cells were purchased from Lonza, subcultured, split into 1 mL aliquots containing 1,000,000 passage three (P3) cells, and frozen in liquid nitrogen prior to use. Endothelial growth media (EGM) was prepared by adding contents of Lonza EGM BulletKit™, which contained 0.5 mL human endothelial growth factor, 0.5 mL hydrocortisone, 0.5 mL acetic acid, 0.5 mL GA-1000 antibiotic antifungal solution, 2 mL bovine brain extract, and 10 mL fetal bovine serum, to endothelial basal media. HUVECs were cultured in EGM, which was replaced every 48 hours, and incubated at 37°C, 5% CO_2. Subculture was conducted using trypsin enzyme, trypsin neutralizer, and a 4-(2-hydroxyethyl)-1-piperazineethanesulfonic acid (HEPES) wash solution containing 25 mM HEPES and 44 mM sodium bicarbonate in phosphate-buffered saline (PBS) prior to 100% confluence, and prior to P7.

2.1.2 Production of Collagen-Functionalized Polyacrylamide Gel Coated Glass Coverslips

Glass 18 x 18 mm coverslips were first activated by undergoing 2 minutes of plasma cleaning, 10 minutes of incubation in *Milli*-Q (MQ) water containing 1% polyethylenimine, three 5 minute MQ water washes, air drying, 30 minutes of incubation on PBS containing 0.1% glutaraldehyde, three 5 minute MQ water washes, and then allowed to air dry.

Polyacrylamide gels were prepared by combining 40% acrylamide, bis-acrylamide, HEPES in MQ water at pH 6, tetramethylethylenediamine (TEMED), and MQ water, adjusting the pH of the solution to 6 using HCl, and degassing the solution to remove oxygen, which would otherwise inhibit polymerization from occurring in a later step. N-6-((acryloyl)amido) hexanoic acid (N6) dissolved in ethanol (EtOH) was added to the solution to enable attachment

of collagen in a later step. PA gel stiffness was controlled by adjusting the ratio of 40% acrylamide to bis-acrylamide, as described previously by our lab and by others.[75,76] Ammonium persulfate (APS) dissolved in MQ water was added to the solution, initiating polymerization, which was then immediately pipetted onto activated square glass coverslips and covered by circular 18 mm diameter glass coverslips coated in Rain-X. Once PA gels were polymerized, circular coverslips were removed, and square glass coverslips coated in PA were inverted onto droplets of 0.1 $mg \cdot ml^{-1}$ rat tail tendon (RTT) collagen type I in 50 mM HEPES solution at pH 8 on flat Parafilm. Following collagen polymerization, gels were inverted onto droplets of 1:1000 ethanolamine in 50 mM HEPES solution at pH 8 on flat Parafilm to cap unreacted N6. Square glass coverslips coated with PA gels functionalized with collagen were washed in PBS, then stored at 4°C in a PBS solution containing 5% Penicillin Streptomycin and 1% amphotericin B until cell seeding. This procedure is similar to one described previously by our lab.[75]

2.1.3 Monolayer Permeability Assay

Square glass coverslips coated with PA gels functionalized with collagen were moved to a sterile laminar flow hood, placed in wells of uncovered 6-well plates containing sterile PBS, and exposed to UV light for 30 minutes. HUVECs suspended in EGM were prepared with a concentration of 50,000 to 100,000 cells per mL, and 2 mL of this solution was added to each PA gel. HUVECs were allowed to form confluent monolayers over a period of 5 to 7 days with media replacement every 48 hours. To some samples, EGM containing PF573228, BAPN, or dimethyl sulfoxide (DMSO) was added 24 hours prior to the start of the assay.

On the day of the assay, a 0.4 $mg \cdot mL^{-1}$ 40 kDa FITC-dextran solution was prepared in EGM. Per seeded PA gel, 4 mL of this solution was added to a 35 mm MatTek glass-bottomed dish, all of which were stored in an incubator at 37°C, 5% CO_2. One at a time, seeded PA gels were transferred to filled MatTek dishes and visualized using a Zeiss LSM700 equipped with a C-Apochromat 40x/1.1 W Corr water immersion objective. Five minutes after submersion in

FITC-dextran solution, a vertical line scan was captured at the center of the seeded PA gel, spanning from 200 μm below the monolayer to 100 μm above the monolayer.

Monolayer permeability was quantified by calculating the normalized intensity ratio (NIR). First, the intensity ratio (IR) was determined by dividing the FITC signal intensity within the gel (below the monolayer) by that within the fluorescent solution (above the monolayer). To produce NIR values, the IR values of seeded PA gels were divided by the IR values of unseeded control PA gels, as previously described by our lab (Figure 1).[45]

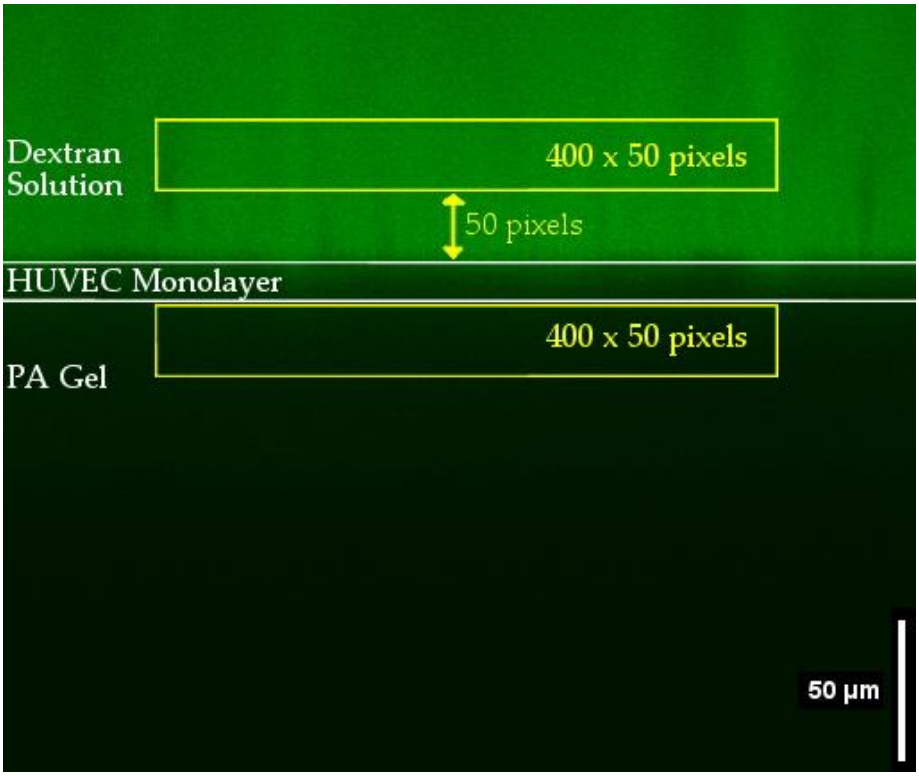

Figure 1: HUVEC-seeded 10 kDa PA gel submerged in FITC-dextran solution. Cell monolayer outlined in white, and regions of interest (ROIs) used in data analysis shown in yellow. IR calculated by dividing the lower ROI intensity by the upper ROI intensity.

2.1.4 HUVEC-Infused Glycated Collagen Gel Preparation

To form "stiff" glycated collagen gels, 150 μL of 10 $mg \cdot mL^{-1}$ RTT collagen type I in 0.1% acetic acid (AA) was mixed with 527 μL of 0.1% AA and 169 μL of 500 mM ribose in 0.1% AA on ice in a laminar flow hood, then incubated at 4°C for 5 days to permit non-enzymatic glycation reactions to occur, leading to the formation of cross-links between collagen fibers. To form "compliant" collagen gels, 150 μL of 10 $mg \cdot mL^{-1}$ RTT collagen type I in 0.1% AA was mixed with 696 μL of 0.1% AA, and also incubated at 4°C for 5 days. After the incubation period, 100 μL of a 10X HEPES buffer solution containing 250 mM HEPEs, 440 mM $NaHCO_3$, and 0.11 $g \cdot L^{-1}$ phenol red in 10X PBS was added to each collagen solution, followed by 4 μL of 1 M NaOH in MQ water, followed by 50 μL of EGM containing 800,000 HUVECs. This produced a HUVEC-infused collagen solution volume of 1 mL, and a final collagen concentration of 1.5 $mg \cdot mL^{-1}$. Compliant collagen gels formed by this method were previously reported to possess a compressive elastic modulus of 175 Pascal, whereas stiff ones were previously reported to possess a compressive elastic modulus of 555 Pascal.[41]

Into wells of a 24-well plate, 300 μL of HUVEC-infused collagen solution was pipetted. These were polymerized via incubation at 37°C, 5% CO_2 for 45 minutes. Polymerized gels were then submersed in 300 μL of EGM and incubated at 37°C, 5% CO_2 for one hour to acclimate. In this time, fresh angiogenic media containing 40 ng·mL VEGF, 40 ng·mL bFGF, 50 ng·mL tetradecanoyl phorbol acetate, and 50 μg·mL ascorbic acid in EGM was prepared.[38] Following the acclimation period, EGM was replaced with angiogenic media, and gels were incubated at 37°C, 5% CO_2 for 24 hours. After the incubation period, gels were transferred to 1.7 mL tubes using a pipetter, immediately flash frozen in liquid nitrogen, and stored at -80°C until further processing. In some cases, 100 μL collagen gels containing 80,000 cells were prepared in 96-well plates, which polymerized in 30 minutes, and which were sustained by 100 μL of media.

2.1.5 Western Blotting Techniques

Per HUVEC-infused glycated collagen gel, a mortar and pestle was washed in alconox, submersed in 70% ethanol, air dried, autoclaved, chilled overnight at -80°C, and then filled with liquid N_2. Each gel was transferred from storage at -80°C to a mortar containing liquid N_2. Immediately following evaporation of liquid N_2, each gel was ground to a fine powder in the presence of 150 μL of 6x Laemmli buffer, which was prepared by mixing 6 mL 4x Tris·Cl/SDS at pH 6.8, 3 mL glycerol, 1 gram sodium dodecyl sulfate (SDS), 0.9 mL β-mercaptoethanol, and 100 μL bromophenol blue. 4x Tris·Cl/SDS was prepared by mixing 12.1 grams 2-Amino-2-(hydroxymethyl)propane-1,3-diol (Tris) and 0.8 grams SDS in 80 mL MQ water, adjusting pH with HCl, adding MQ water to obtain a volume of 200 mL, and then filtering through a 0.45 μm filter. Grinding continued until a liquid solution formed, which was poured into a 1.7 mL tube and stored at -80°C until use in a western blot.

Four running gels were prepared by mixing 8.4 mL 30% acrylamide/bis and 7.875 mL 4x Tris·Cl/SDS at pH 8.8 with 15.225 mL MQ water, and then degassed for at least 30 minutes. While degassing, the Mini-PROTEAN® casting apparatus was assembled per Bio-Rad's instructions, with glass plates separated by 1.5 mm.[77] Following degassing, 21 μL TEMED and 105 μL 10% APS in MQ water were added to the solution, and 7.4 mL of solution per gel was pipetted between glass plates. Gels were immediately covered with 0.5 mL water-saturated isobutyl alcohol and allowed to polymerize for 45 minutes. In this time, running and -20°C transfer buffers were prepared from 10x stock solutions, as described in Bio-Rad's protocol.[77]

Four stacking gels were prepared by mixing 1.95 mL 30% acrylamide/bis and 3.75 mL 4x Tris·Cl/SDS at pH 6.8 with 9.15 mL MQ water, and then degassed for at least 15 minutes. While degassing, water-saturated isobutyl alcohol was removed from polymerized running gels. Following degassing, 15 μL TEMED and 75 μL 10% APS in MQ water were added to the solution, and 3 mL of solution per gel was pipetted between glass plates over polymerized

running gel. Combs were inserted into stacking gels, which were allowed to polymerize for 30 minutes. In this time, samples were thawed and heated to 95°C for 5 minutes.

Once polymerized, combs were removed from the stacking gel, leaving behind wells. Gels sandwiched between glass plates were removed from casting apparatus and assembled into running apparatus, to which running buffer was added, per Bio-Rad's instructions.[77] Each well was filled with either 5 μL Kaleidoscope™ Prestained SDS-PAGE Standards ladder (Bio-Rad Laboratories), 30 μL sample, or 5 μL 6x Laemmli buffer. Subsequently, electrophoresis was conducted at 100 volts for approximately 105 minutes.

Following electrophoresis, protein-infused running gel was removed from running apparatus and glass plates, cut away from the separating gel, and submerged in chilled transfer buffer for at least 5 minutes. In this time, a polyvinylidene difluoride (PVDF) membrane was wetted in methanol for 30 seconds, and rocked in chilled transfer buffer for 5 minutes. Once acclimated, the protein-infused running gel and PVDF membrane were placed within assembled separating apparatus per Bio-Rad's instructions.[78] Subsequently, electrophoresis was conducted within a cold room at 34 volts for 14 hours.

Following transfer of proteins from running gel to PVDF membrane, separating apparatus was disassembled, and membranes were air dried for 30 minutes. In this time, TBS-t solution was prepared by mixing 899 mL MQ water with 1 mL Polysorbate 20 and 100 mL 10x Tris-buffered saline (TBS) solution, which itself was 100 mM Tris, 1500 mM NaCl in MQ water at pH 7.8. Dried membranes were cut and labeled, then wetted in methanol for 30 seconds, then washed twice in TBS-t for 10 minutes. In this time, blocking solutions of 5% bovine serum albumin (BSA) in TBS-t or 5% milk in TBS-t were prepared. Following washes, membranes were rocked at room temperature for one hour or overnight at 4°C.

Primary antibodies (1°abs) were prepared at 1:2000 dilution in 5% milk in the case of Glyceraldehyde 3-phosphate dehydrogenase (GAPDH), a housekeeping protein, or at 1:1000 dilution in 5% BSA in all other cases. Blocked membranes were placed within sealed plastic bags containing 3 mL of 1°ab solution, and rocked overnight at 4°C. The next day, 2°abs conjugated to horseradish peroxidase were prepared at 1:2000 dilution in the appropriate blocking solution while membranes underwent four TBS-t washes. Washed membranes were placed within sealed plastic bags containing 3 mL of 2°ab solution, and rocked for one hour at room temperature. Following that, membranes underwent four TBS-t washes.

Proteins within membranes were imaged using West Pico, Dura, or Femto, per their respective protocols, using an ImageQuant™ LAS-4000.[79–81] Images were analyzed using the gel analysis tool contained within imageJ: Analyze → Gels → Select First Lane applied to a square ROI around the first protein band, Select Next Lane applied to square ROIs around all subsequent bands (Figure 2A). Per protein band, a histogram was generated via Analyze → Gels → Plot Lanes, background was excluded from the peak via the line tool, and the total protein band signal was obtained via the tracing tool (Figure 2B).

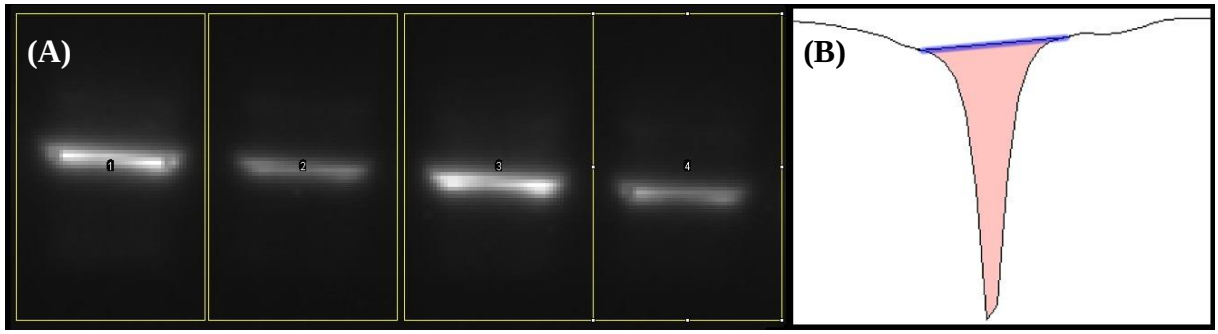

Figure 2: (a) Protein bands surrounded by ROIs used in the Analyze → Gels tool within imageJ. Brightness and contrast enhanced here to aid in visualization of the technique. (b) Histogram of the first band generated by the Analyze → Gels tool with background cut away (blue line) and total protein band signal selected (red highlight).

To re-use membranes for the visualization of protein bands with similar molecular weights, four TBS-t washes, a 15 minute wash in Restore™ Western Blot Stripping Buffer (Thermo Fisher Scientific), four additional TBS-t washes, and incubation in blocking solution were conducted prior to the application of additional primary and secondary antibodies.

Primary antibodies used in this study includes those for GAPDH (BioLegend, Poly6414), FAK (Cell Signaling Technology, 3285S), phospho-FAK-Y397 (Cell Signaling Technology, 3283S), Src (Cell Signaling Technology, 2108S), phospho-Src-Y418 (EMD Millipore, 07-909), VE-cadherin (Santa Cruz Biotechnology, sc-52751), and phospho-VE-cadherin-Y685 (EMD Millipore, AB1955). Anti-rabbit and anti-mouse secondary antibodies were conjugated to horseradish peroxidase.

2.2 *Ex Ovo Techniques*

2.2.1 Chicken Embryo Culture

White Leghorn chicken eggs supplied by the Cornell Poultry farm, reachable at phone number (607) 272-8970, were cleaned of debris using a dry cloth and stored in a wine cooler at 12.8°C on ED0 prior to transfer to a GQF 1500 Professional rocking egg incubator maintained at 37.8 ^{0}C, 60% relative humidity. On ED3, eggs were cracked and plied open within a laminar flow cabinet using a c-clamp and a hacksaw (Figure 3A). Egg contents were transferred into *ex ovo* culture platforms, which were constructed by slinging a single layer of AEP PVC wrap over a 5 oz. Fineline Savvi Serve™ cup partially filled with warm water (Figure 3B). A small scoop of autoclaved ground eggshell was distributed around the albumin, and culture platforms were capped with a Petri dish lid. Chicks within culture platforms were incubated in Hova-Bator circulated air incubators maintained at 37.8 ^{0}C, 55% relative humidity.

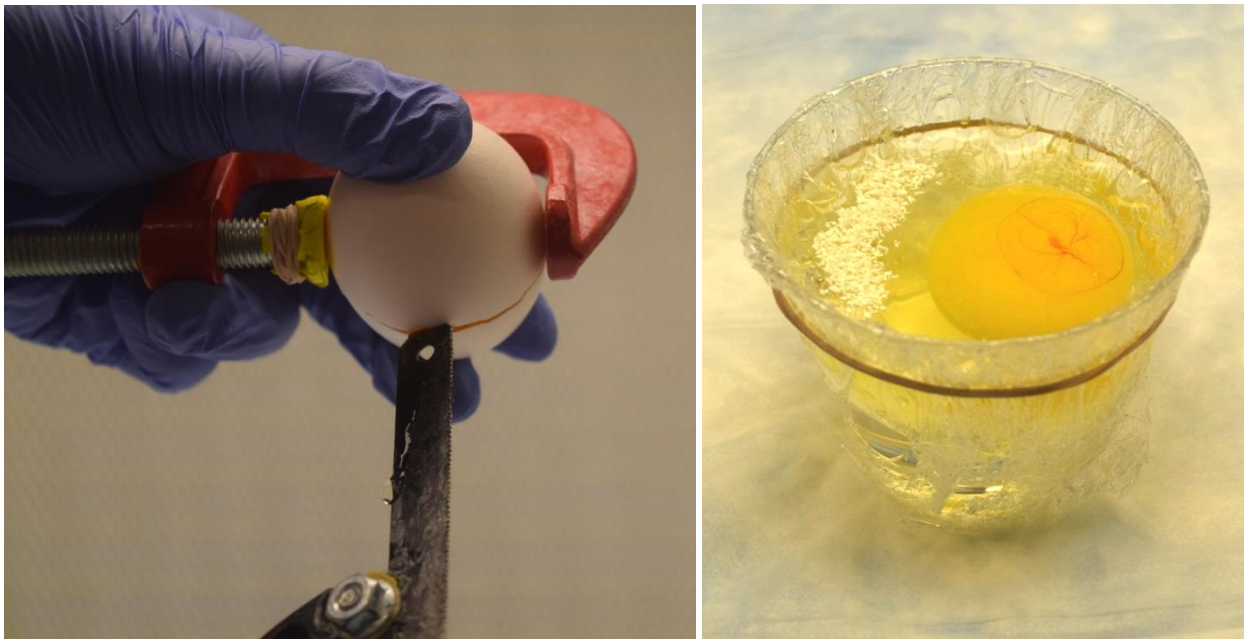

Figure 3: (a) Eggs were slightly squeezed using a c-clamp, then tapped with a hacksaw to form a crack. The crack was plied open using the hacksaw tip until albumin began leaking, at which point the egg was removed from the c-clamp and pulled apart over an *ex-ovo* culture platform. (b) E*x-ovo* culture platform containing living chicken embryo and sterile ground eggshells.

2.2.2 Construction and Grafting of Collagen Constructs

As in section 2.1.4, stiff glycated collagen construct formation began with the mixing of 150 µL of 10 mg·mL^{-1} RTT collagen type I in 0.1% AA with 527 µL of 0.1% AA and 169 µL of 500 mM ribose in 0.1% AA on ice in a laminar flow hood, followed by incubation at 4°C for 5 days to permit non-enzymatic glycation reactions to occur. Likewise, compliant collagen construct formation began with the mixing of 150 µL of 10 mg·mL^{-1} RTT collagen type I in 0.1% acetic acid with 696 µL of 0.1% AA, followed by an incubation at 4°C for 5 days. After the incubation period, 100 µL of 10X HEPES buffer solution and 4 µL of 1 M NaOH in MQ water were added to each solution. At this point, solutions were infused with RH VEGF 165 (R&D Systems) and bFGF (PeproTech) to generate concentrations of 5 µg·mL^{-1} and 16.7 µg·mL^{-1} respectively, which have previously been shown to induce angiogenic ingrowth into collagen gels.[73] Select solutions were also infused with MT1-MMP inhibitor GM6001 to generate a concentration of 5 µM, which was found by our lab to inhibit the angiogenic outgrowth of endothelial cell spheroids.[82] AA was then added to solutions to produce a final volume of 1 mL.

Onto autoclaved nylon mesh squares with edge lengths approximating five millimeters, 30 μL of collagen solution was pipetted, which was immediately sandwiched by another nylon mesh square. Sandwiched collagen was then polymerized for 30 minutes via incubation at 37°C, 5% CO_2. Immediately following incubation, constructs were placed on the CAMs of ED10 chicken embryos in a laminar flow cabinet (Figure 4). Chicken embryos were immediately returned to their incubators following the procedure.

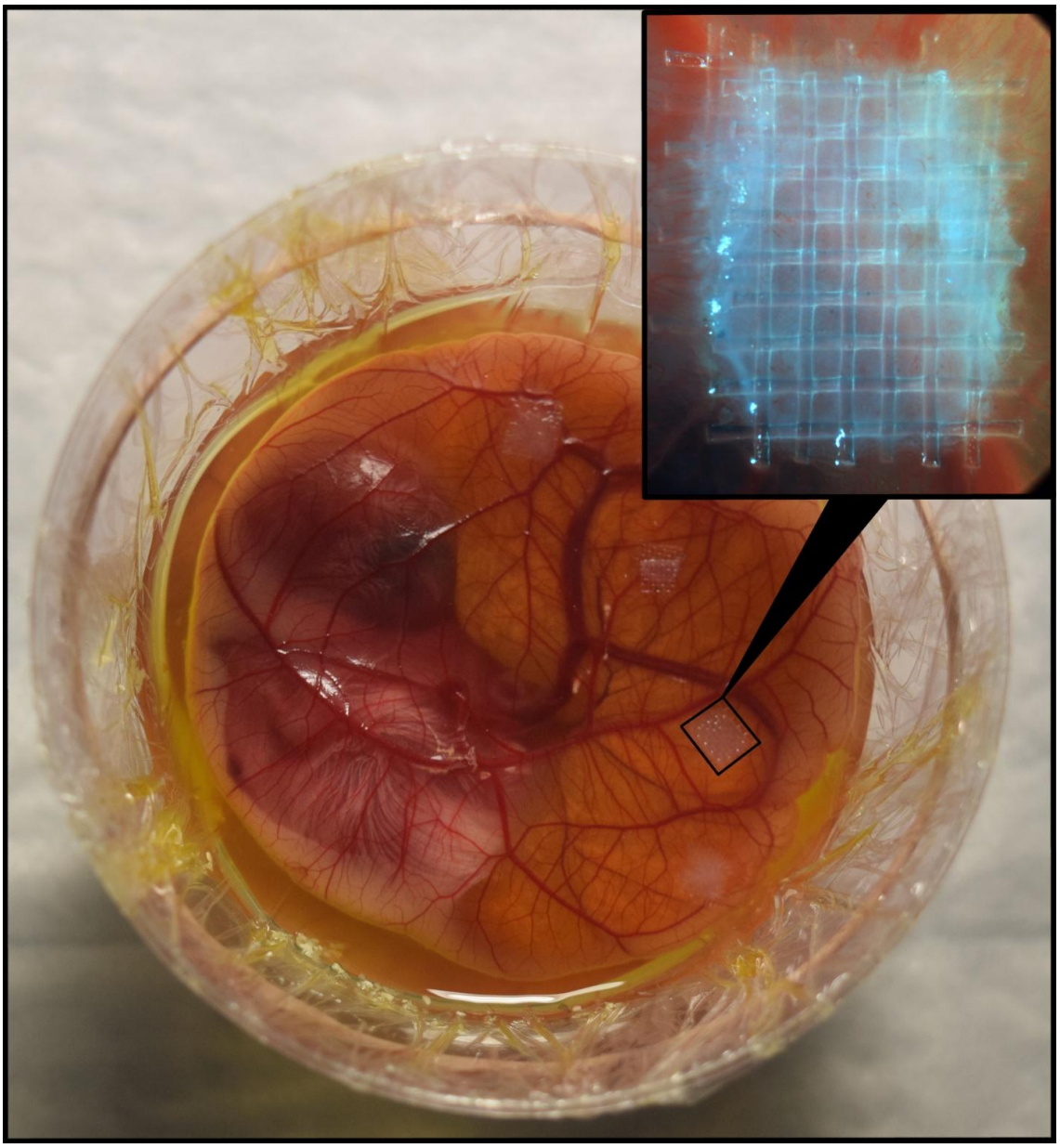

Figure 4: Chicken embryo to which has been grafted four collagen constructs (expanded). Expanded image taken using a Zeiss steREO Discovery.V8 scope.

2.2.3 Angiogenic Vascularization Assay

On ED13, chicken embryos cultured *ex ovo* were placed under a Zeiss steREO Discovery.V8 scope. As described previously by Nguyen *et. al.*, lens focus was placed on the vessels above the bottom mesh, and vascular density was defined as the percentage of mesh squares containing vessels.[83] Peripheral squares were not considered, nor were those under which the bottom mesh or collagen gel was not visibly present.

2.2.4 Neovessel Permeability Assay

To preface this section: collagen constructs destined for use in the neovessel permeability assay were not formed with a top mesh. On ED15, chicken embryos cultured *ex ovo* were transferred from hammock-styled platforms to Petri dishes. Proximal vessels were injected with 100 µL of dye solution containing 2.5 $mg \cdot mL^{-1}$ 65-85 kDa TRITC-dextran (T1162, Sigma-Aldrich) and 2.5 $mg \cdot mL^{-1}$ 2 MDa FITC-dextran (FD2000S, Sigma-Aldrich) in PBS. Neovessels within collagen constructs were visualized using two-photon microscopy on a Zeiss LSM 880 upright equipped with a EC Plan-Neofluar 10x/0.3 objective and a Mai Tai laser with a wavelength of 900 nm. Fluorescent z-stacks of neovessels, which were identified using the FITC-dextran, were taken approximately every 15 minutes for one hour (Figure 5).

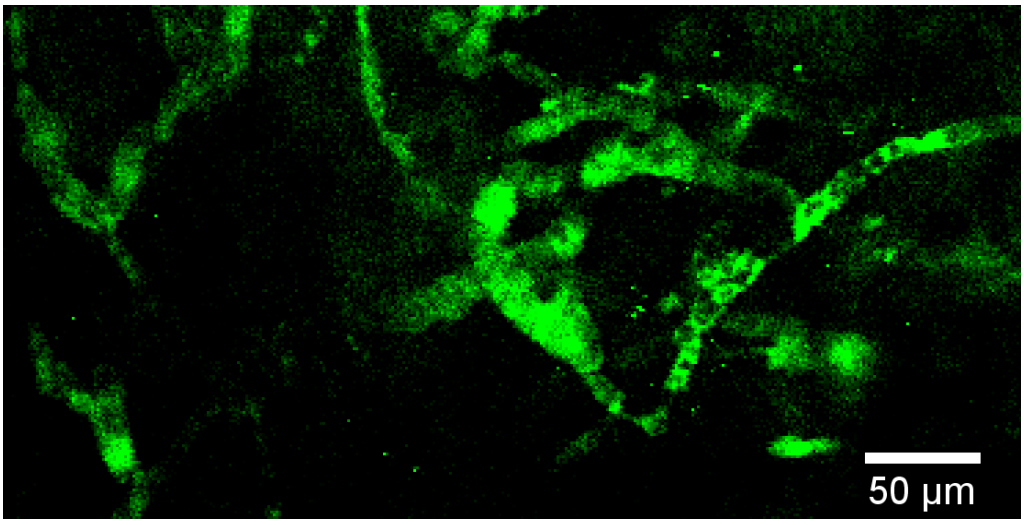

Figure 5: 2 MDa FITC-dextran fluorescent signal flowing through neovessels grown within a compliant collagen construct 30 minutes post-injection.

Quantification of neovessel permeability began by plotting the fluorescent intensity of the TRITC signal across a 20 pixel thick line perpendicular to the neovessel of interest at each time point. Intensity values were normalized to the peak value per plot, and peaks were aligned across all time points. Then, the integrals under each peak were calculated and plotted as a function of time. Neovessel permeability was then defined as the rate of increase of the integral of the normalized fluorescent intensity signal (Figure 6). This method was adapted from a paper that quantified vascular permeability of large CAM vessels in response to drug administration.[84]

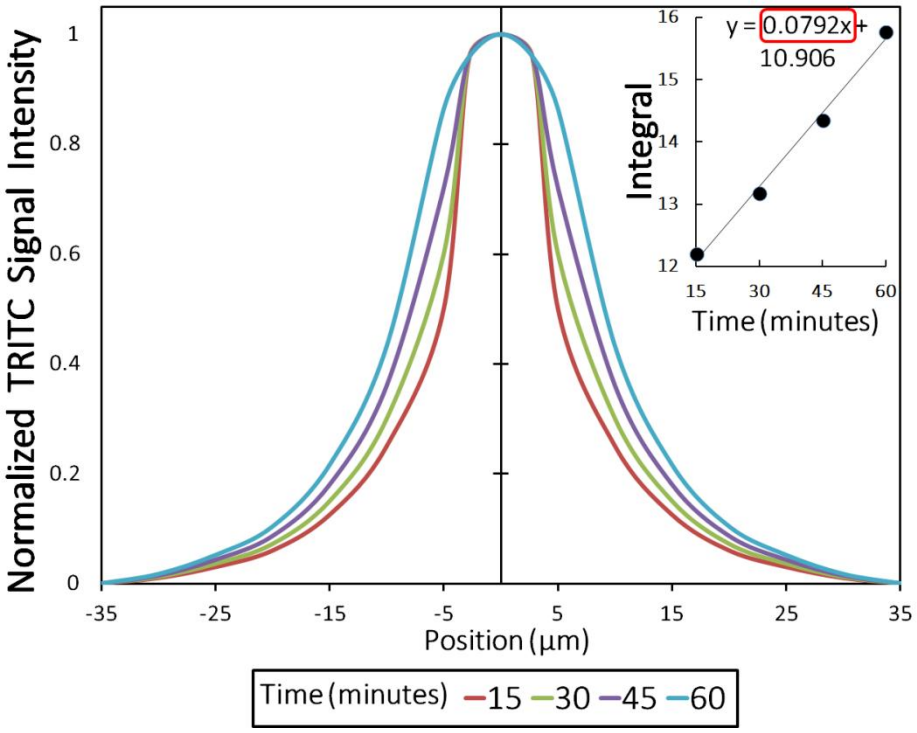

Figure 6: Depiction of neovessel permeability data analysis. At each time point, the intensity of the TRITC signal was recorded as a function of position along the ROI, and normalized to the peak intensity value, which occurred within the neovessel. Then, the integral under each curve was calculated. Neovessel permeability was then defined as the rate of increase of the integral (outlined in red in this example).

CHAPTER 3

RESULTS

3.1 Matrix Stiffening Promotes Vascularization in an MT1-MMP Dependent Manner

We hypothesized that increasing the stiffness of a tissue's extracellular matrix would increase the extent of angiogenic vascularization it experiences. To test our hypothesis, we grafted compliant and stiff collagen constructs to the CAMs of chicken embryos cultured *ex ovo*. Apart from glycation induced by addition of ribose, constructs of varying stiffness type were identical. Three-days post-grafting, neovessels within the constructs were readily visible (Figure 7A), and the percentage of mesh squares containing neovessels was quantified. We found that cross-linked collagen gels contained significantly more neovessels than their compliant counterparts, shown by an increase in vascular density from 47% ± 6% to 72% ± 5%, suggesting that matrix stiffening promotes angiogenic vascularization (Figure 7B). To identify whether AGEs were responsible for the increase in vascular density observed in stiff constructs, parallel experiments were conducted in which glutaraldehyde was used as a cross-linking agent. Still, we found that vascularization significantly increases within gels containing cross-linked fibers. This finding was supported by the data of others within the lab, which revealed that extensions from HUVEC spheroids embedded within glycated collagen gels were more numerous, longer, and consisted of more branching points than those within untreated collagen gels, and by additional data indicating that mouse tumors softened with BAPN contained fewer vascular branches per image field than did untreated tumors.[82]

To investigate the role that MT1-MMP activity plays in stiffness-dependent angiogenic vascularization, we infused select constructs with 5 mM GM6001 prior to gel polymerization. Analysis of the constructs revealed that inhibition of MMP activity via chelation of the active site zinc atom eliminates the stimulating effect that increasing matrix stiffness has on angiogenic vascularization, but does not significantly influence compliant gels (Figure 7B).[85]

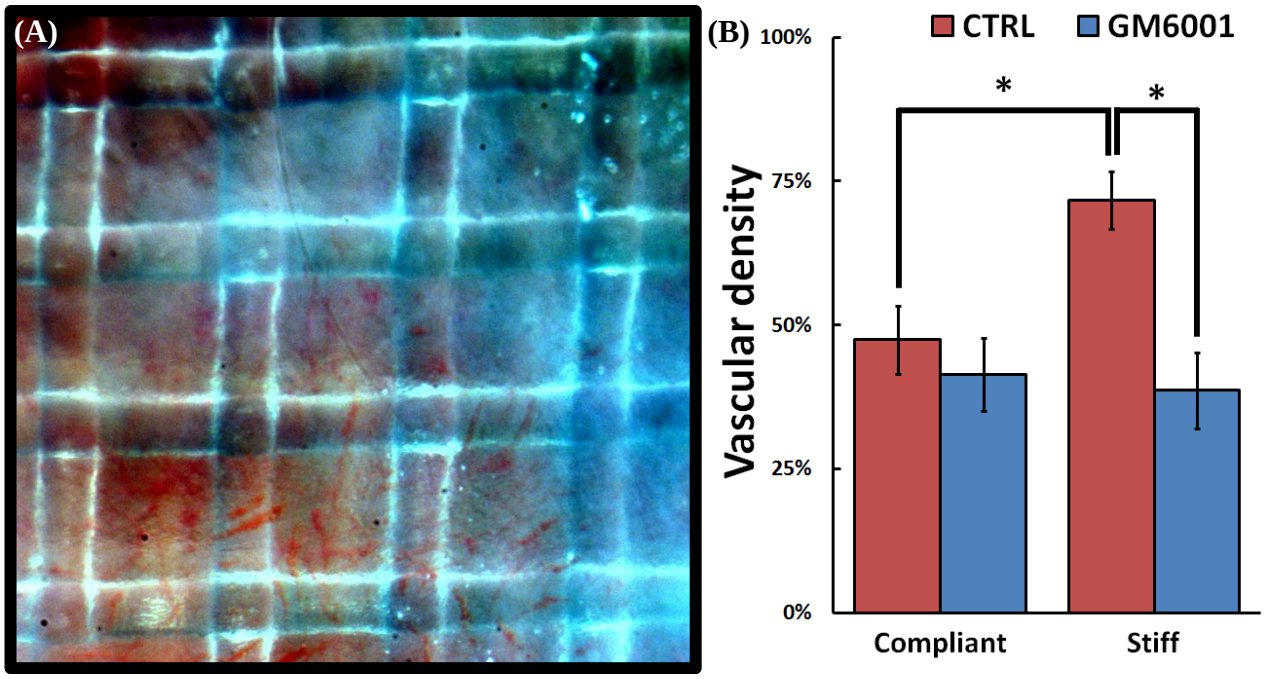

Figure 7: (a) Image of neovessels within a construct occupying five out of nine mesh squares. (b) Vascular density as a function of collagen cross-linking via glycation with 0 or 100 mM ribose, and of GM6001 inclusion (n_{total} = 80). Data presented as mean ± standard error, with* indicating $P < 0.05$.

3.2 Matrix Stiffening Induces Vascular Permeability

We hypothesized that increasing the stiffness of the extracellular matrix in contact with the endothelial monolayer would increase its permeability. To test this hypothesis, we formed HUVEC monolayers on collagen-functionalized polyacrylamide gels with elastic moduli of 2.5 kPa and 10 kPa. Monolayer permeability was assessed by placing the PA gels within glass-bottomed dishes containing 4 mL of EGM with 0.4 $mg \cdot mL^{-1}$ 40 kDa FITC-dextran, which was selected because its hydrodynamic radius is similar to that of albumin, which has been used by other labs to evaluate permeability.[45] We found that increasing substrate stiffness by four-fold increased HUVEC monolayer permeability, represented by an increase in the normalized intensity ratio, by 80%, from 0.49 ± 0.016 to 0.88 ± 0.028 (Figure 8A).

Having identified that increasing the stiffness of a 2D substrate increases the permeability of the HUVEC monolayer formed on it, we hypothesized that increasing the stiffness of a 3D tissue would increase the permeability of the microvasculature within it. To test our hypothesis, we adapted a modified version of a technique used to evaluate the effect that systemic drugs have on the permeability of large CAM vessels, previously described by Pink *et. al.*, to quantify the permeability of angiogenic neovessels within glycated collagen constructs.[84] Briefly, ED15 chicken embryos were injected with 100 μL of 2.5 $mg \cdot mL^{-1}$ 2 MDa FITC and 65-85 kDa TRITC dextran, neovessels within collagen constructs were visualized, and z-stacks were taken approximately every 15 minutes. Then, TRITC signal intensity as a function of position across the neovessel data was acquired at each time point, and normalized to the peak intensity value found within the neovessel, and the integral of each of these curve was calculated. Then, vascular permeability was defined as the rate of increase of the integrals. Following analysis, we found that cross-linking collagen fibers via non-enzymatic glycation, which yields a three-fold increase in matrix stiffness, increased permeability by approximately 46% (Figure 8B).

To validate our neovessel permeability assay, and to ensure that extravasation of the TRITC-signal was not saturated, positive control samples were generated by adding 500 ng of VEGF to select injection mixtures, which produced a circulating VEGF concentration of approximately 225 $ng \cdot mL^{-1}$, which is between four and five times the concentration typically used to induce hyperpermeability *in vitro*.[86,87] As expected, we found that administration of VEGF significantly increased neovessel permeability despite matrix stiffness (Figure 8B).

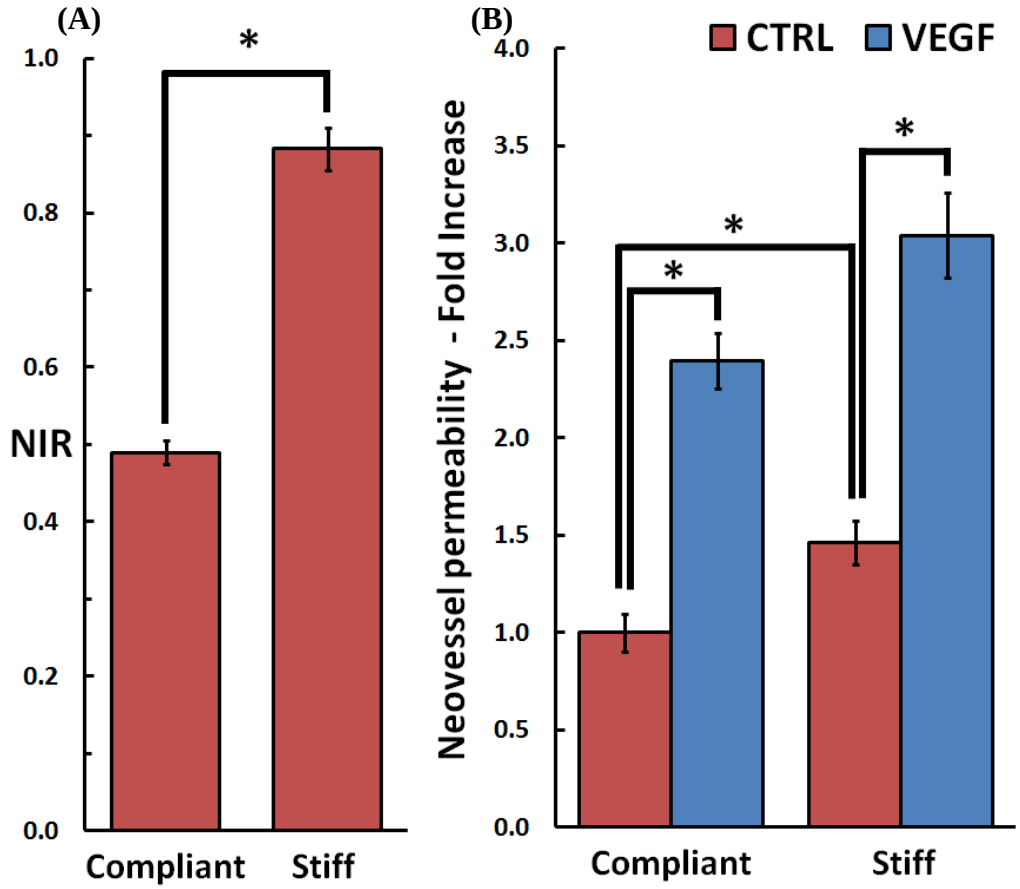

Figure 8: (a) Normalized intensity ratio of HUVEC monolayers seeded on compliant (2.5 kPa) and stiff (10 kPa) PA gels (n_{total} = 47). (b) *Ex ovo* neovessel permeability assay as a function of collagen cross-linking via glycation with 0 or 100 mM ribose, and of VEGF inclusion (n_{total} = 70). Data presented as mean ± standard error, with * indicating $P < 0.05$.

3.3 FAK Inhibition Normalizes the Integrity of Leaky Neovessels Within Stiff Tissues

Having identified that matrix stiffness influences vascular permeability, we sought to normalize the integrity of leaky neovessels within stiff tissues. Within tumor samples of various cancer types, FAK overexpression has been linked to poor patient prognosis, and FAK Y397 phosphorylation has been correlated to tumor stiffening and progression.[59] In addition to mediating VEGF-induced hyperpermeability, FAK Y397 phosphorylation has been shown to directly phosphorylate VE-cadherin Y658, which disrupts junction integrity.[54,57,63,64] FAK Y397 phosphorylation also has the potential to indirectly influence permeability via regulation of Rho-family GTPases, Src, and VE-cadherin accessory molecules.[51,57] For this reason, we chose to evaluate the effect that FAK Y397 inhibition has on permeability *in vitro* and *ex ovo*. To achieve this, PF573228, a small-molecule that interacts with FAK at the ATP-binding pocket with an IC_{50} of 4 nM in enzyme suspension and 30 nM to 100 nM in cell culture, was employed.[69]

To the media sustaining HUVEC monolayers seeded on compliant (2.5 kPa) and stiff (10 kPa) PA gels, PF573228 was added 24 hours prior to data collection to produce concentrations of 4, 40, 100, and 200 nM. Interestingly, while we found that FAK inhibition produced no significant change in the permeability of monolayers formed on compliant substrates, it significantly reduced the permeability of those grown on stiff substrates at concentrations of 40 nM, 100 nM, and 200 nM (Figure 9A).

To evaluate the effect that FAK inhibition has on permeability *ex ovo*, 30 μL MQ water containing 1 μM PF573228 was topically applied to collagen constructs 24 hours prior to data collection. Not surprisingly, we found that treatment with PF573228 had no significant effect on the permeability of neovessels within compliant matrices (Figure 9B). Surprisingly, however, it reduced the permeability of neovessels within stiff constructs to compliant construct levels, suggesting that FAK activity is essential to stiffness-induced hyperpermeability (Figure 9B).

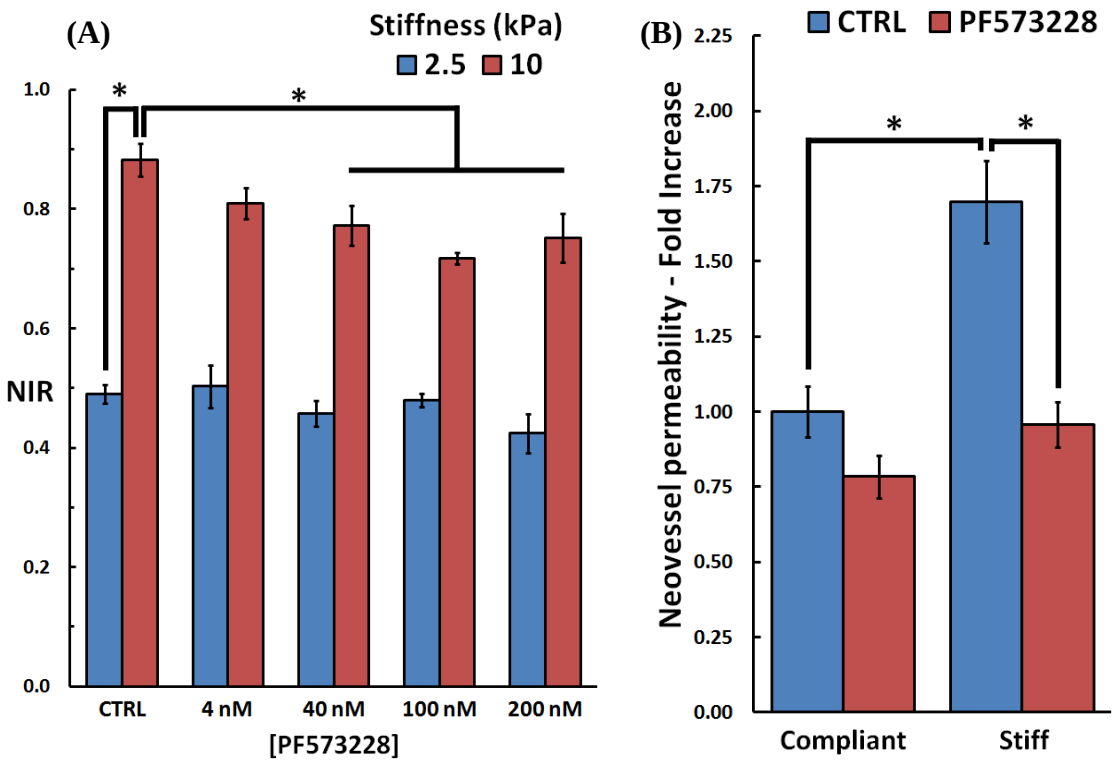

Figure 9: (a) Normalized intensity ratio of HUVEC monolayers seeded on compliant (2.5 kPa) and stiff (10 kPa) PA gels as a function of PF573228 concentration; 40, 100, and 200 nM PF573228 significantly reduce monolayer permeability on stiff PA gels (n_{total} = 118). (b) *Ex ovo* neovessel permeability assay as a function of collagen cross-linking via glycation with 0 or 100 mM ribose, and of topical PF573228 application (n_{total} = 86). Data presented as mean ± standard error, with * indicating $P < 0.05$.

3.4 Role of FAK and Src Activity in Stiffness-Induced Vascular Permeability

Having identified that neovessels grown within stiff cross-linked collagen constructs exhibited elevated vascular permeability relative to those grown in compliant constructs, and that inhibiting FAK Y397 phosphorylation disrupts this effect, we decided to investigate the mechanism responsible. To achieve this, HUVECs were infused within neutralized collagen solutions containing ribose at a concentration of 0 or 100 mM, then polymerized within wells of a culture plate. Immediately following polymerization, gels were acclimated in EGM for one hour, which was subsequently replaced with EGM containing angiogenic growth factors. Samples were incubated for 22 hours, at which point angiogenic media was exchanged with that infused with PF573228 to produce a concentration of 100 nM, and then incubated for two hours.

Following incubation, samples were flash frozen, homogenized via grinding with mortars and pestles in the presence of 6x Laemmli buffer, and then subjected to western blotting techniques. Three independent sets of HUVEC-infused glycated collagen gels were prepared, with each set containing four conditions: compliant control, compliant with PF573228, stiff control, and stiff with PF573228, represented by (C) CTRL, (C) PF, (S) CTRL, and (S) PF.

To evaluate the effect that matrix stiffness has on FAK expression and phosphorylation, and to verify that PF573228 functioned as intended, samples were first analyzed using anti-phospho-FAK-Y397 and anti-FAK antibodies (Figure 10A). Though the low intensity of the protein bands derived from samples infused with PF573228 made it apparent that the FAK inhibitor functioned as intended, we were uncertain whether or not matrix stiffness influenced FAK in any way. Therefore, a densitometric analysis was conducted to quantify the amount of protein present within each band. Total band signal values of each band were normalized to GAPDH, and the fold increase relative to the compliant control sample was plotted (Figure 10B). Furthermore, the ratio of phosphorylated FAK to total FAK was calculated, and the fold increase relative to the compliant control sample was plotted (Figure 10C). To our surprise, it became clear that matrix stiffness does not significantly influence FAK expression or activity.

Based on this finding, we decided to investigate the effect that matrix stiffness and treatment with PF573228 has on the phosphorylation of Src Y418. This specific tyrosine residue was selected, because its phosphorylation is known to trigger the phosphorylation of VE-cadherin tyrosine residues 658 and 685, which are mediators of vascular permeability.[51,56,88] To achieve this, the same samples were analyzed using anti-phospho-Src-Y418 and anti-Src antibodies (Figure 11A). Because it was not immediately clear whether matrix stiffness or FAK inhibition significantly influenced Src expression or phosphorylation, densitometric analysis was conducted, normalized to GAPDH, compared to the compliant control samples (Figure 11B), and the ratio of phosphorylated Src to total Src was calculated (Figure 11C). Interestingly, from this analysis it became clear that while PF573228 does not influence Src expression or activity, increases in matrix stiffness significantly affect the phosphorylation of Src tyrosine residue 418.

Furthermore, we decided to investigate the effect that matrix stiffness and FAK inhibition have on the phosphorylation of VE-Cadherin Y685. To achieve this, samples were analyzed using anti-phospho-VE-cadherin Y685 and anti-VE-cadherin antibodies (Figure 12A). Upon conducting densitometric analysis (Figure 12B) and calculating the ratio of phosphorylated protein (Figure 12C), we were able to determine that increasing matrix stiffness significantly increases VE-cadherin phosphorylation within our system. Furthermore, we were also able to determine that treatment with PF573228 significantly reduces VE-cadherin phosphorylation.

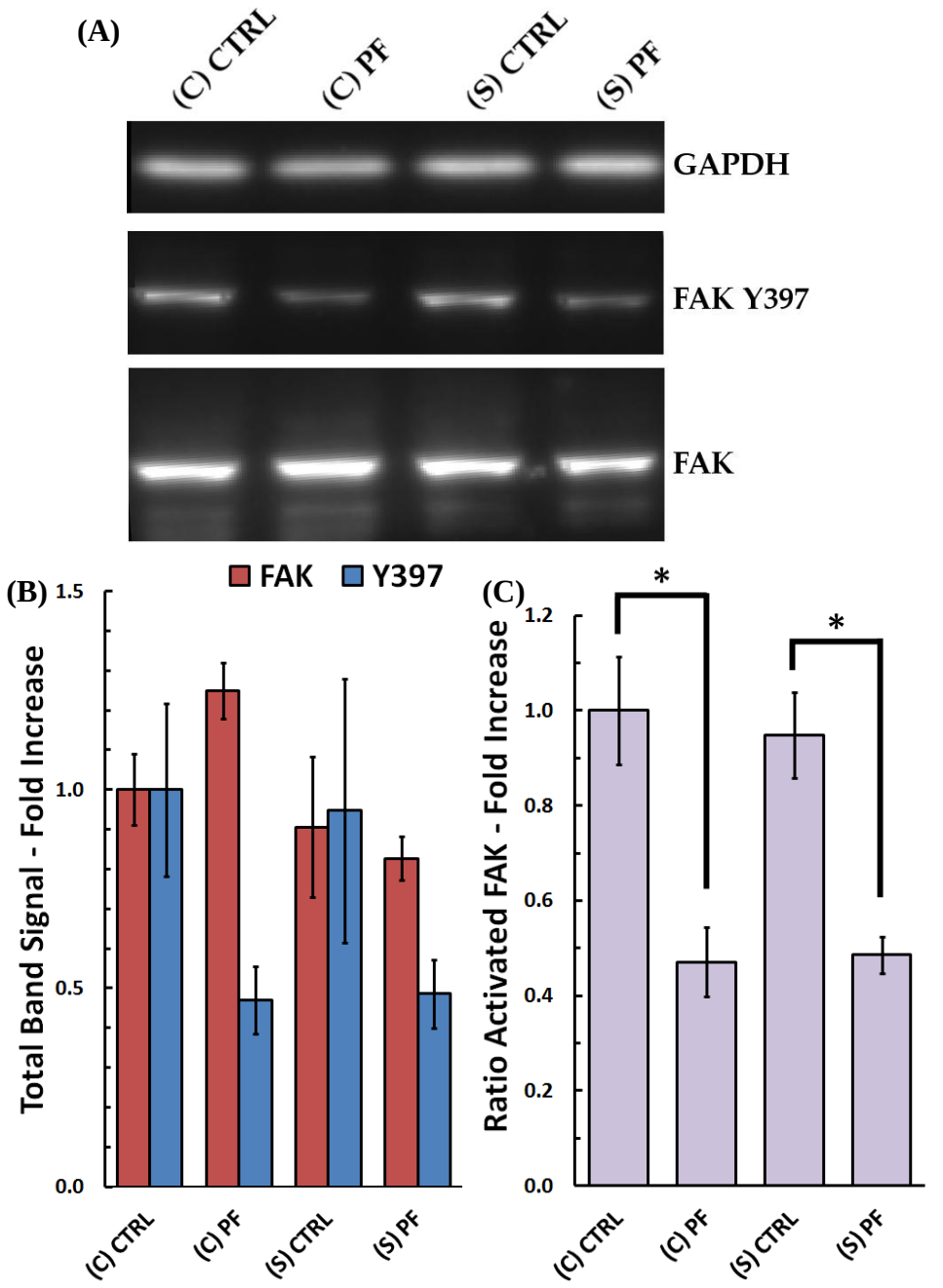

Figure 10: (a) Representative protein bands generated by western blots. (b) Fold increase of total band signal calculated by densitometric analysis. (c) Ratio of phosphorylated FAK Y397 (activated FAK) to total FAK. (S) is stiff gel; 100 mM ribose, (C) is compliant gel; 0 mM ribose PF indicates inclusion of 100 nM PF573228, CTRL indicates no inhibitor. FAK and FAK Y397 total band signal data normalized to GAPDH.
Data presented as mean ± standard error, with * indicating $P < 0.05$.

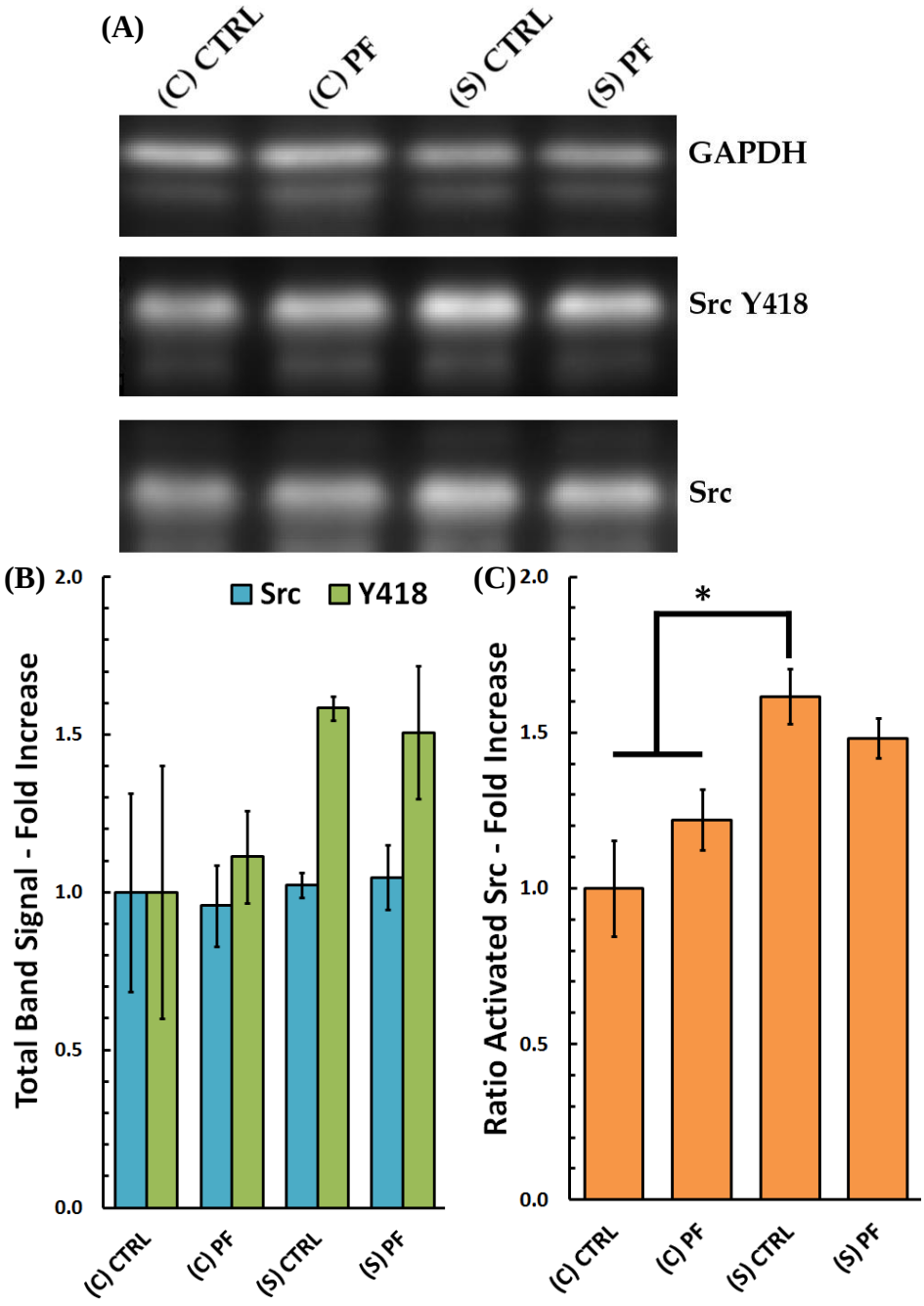

Figure 11: (a) Representative protein bands generated by western blots. (b) Fold increase of total band signal calculated by densitometric analysis. (c) Ratio of phosphorylated Src Y418 (activated Src) to total Src. (S) is stiff gel; 100 mM ribose, (C) is compliant gel; 0 mM ribose PF indicates inclusion of 100 nM PF573228, CTRL indicates no inhibitor. Src and Src Y418 total band signal data normalized to GAPDH.
Data presented as mean ± standard error, with * indicating $P < 0.05$.

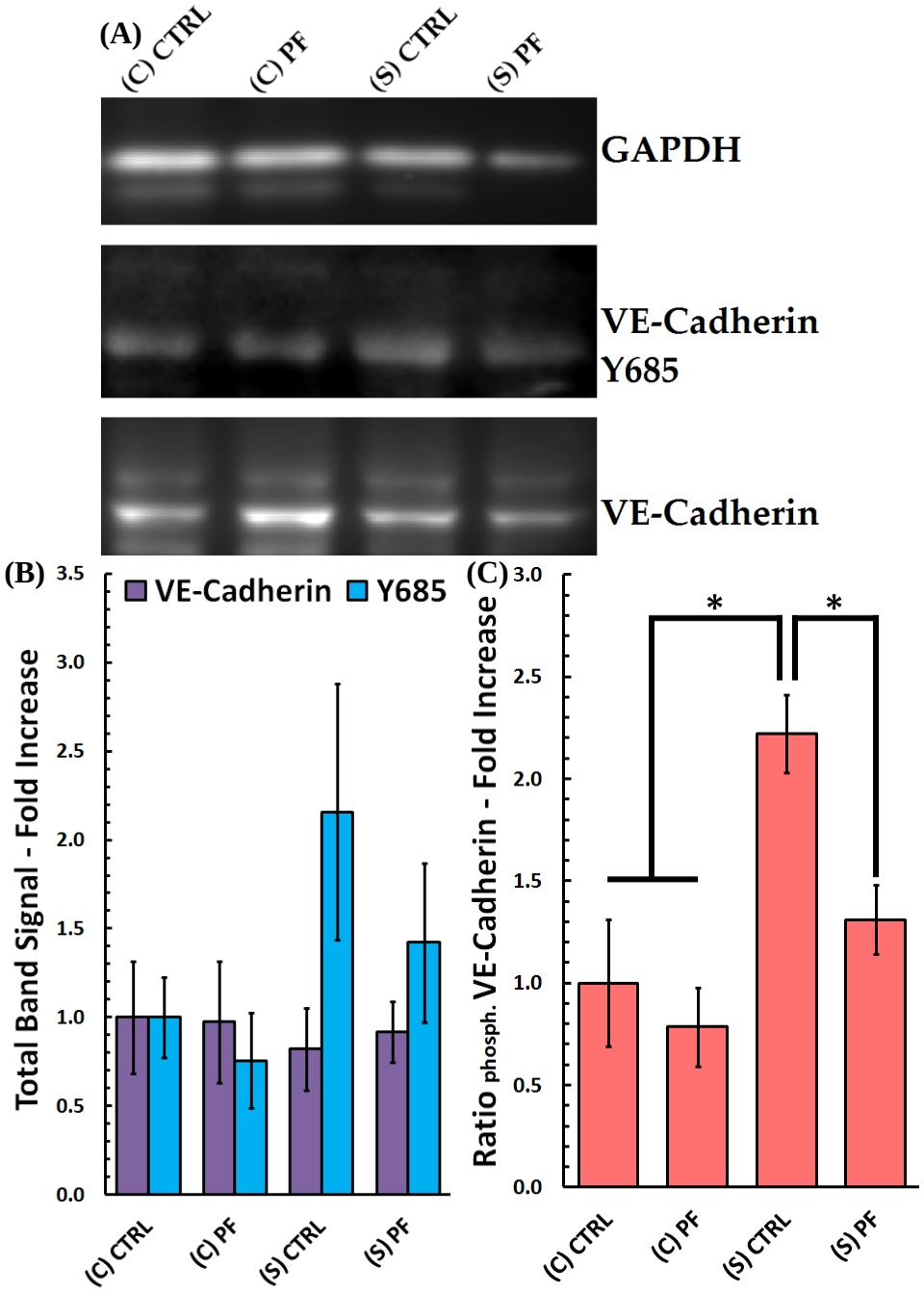

Figure 12: (a) Representative protein bands generated by western blots. (b) Fold increase of total band signal calculated by densitometric analysis. (c) Ratio of phosphorylated VE-Cadherin Y685 to total VE-Cadherin. (S) is stiff gel; 100 mM ribose, (C) is compliant gel; 0 mM ribose PF indicates inclusion of 100 nM PF573228, CTRL indicates no inhibitor. VE-cadherin and Y685 total band signal data normalized to GAPDH. Data presented as mean ± standard error, with * indicating $P < 0.05$.

3.5 Additional Experiments

Additional experiments were conducted to support the work of others complementary my investigation into the effect that matrix stiffness has on vascular permeability. Others in the lab have shown that increases in matrix stiffness produce increases in vascular permeability via an Evan's blue extravasation assay on spontaneous mammary tumors allowed to stiffen by natural means, and on tumors treated with β-aminopropionitrile. BAPN is a widely used inhibitor of lysyl oxidase, and treatment with the drug prevents further collagen cross-linking from occuring.[89,90] Though our findings indicated that treatment with BAPN significantly reduces vascular permeability, we could not claim that this effect was due to a change in matrix stiffness without considering the possibility of it directly affecting endothelial cells. Therefore, we evaluated the effect that treatment with 50 $ng \cdot mL^{-1}$ and 100 $ng \cdot mL^{-1}$ BAPN has on the permeability of HUVEC monolayers grown on stiff (10 kPa) PA gels relative to control samples. These concentrations were selected based on the result of a qualitative cell viability assay. We found that treatment with BAPN had no effect on monolayer permeability (Figure 13).

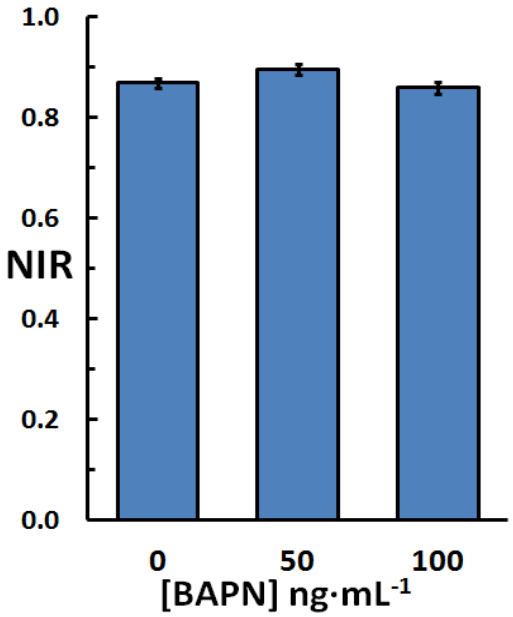

Figure 13: Normalized intensity ratio of HUVEC monolayers seeded on 10 kPa PA gels as a function of BAPN concentration, which was found to have no significant effect on permeability (n_{total} = 66). Data presented as mean ± standard error, with * indicating $P < 0.05$.

Having identified that inhibition of MT1-MMP activity prevents stiffness-induced increases in angiogenic outgrowth, our lab decided to investigate the role that matrix stiffness plays in MT1-MMP expression and activity. In support of this work, and to verify that our MT1-MMP inhibitor functioned as intended, we generated three independent sets of HUVEC-infused glycated collagen gels, with each set containing sixteen gels, four per each of the following conditions: compliant control, compliant with GM6001, stiff control, and stiff with GM6001. We helped process these gels in preparation for western blotting experiments, which a colleague ran to show that increasing matrix stiffness enhances both MT1-MMP expression and activity. Additional gels were prepared for use in an EnSens MMP-14 activity detection kit assay, which enabled fluorescent visualization of MT1-MMP activity in live cells via the addition of a molecular rotor dye and a substrate containing a dye binding site hidden by a cleavable unit.[91,92] These samples were imaged using an Zeiss LSM 880 inverted equipped with a C-Apochromat 40x/1.2 W Corr M27 water immersion objective (Figure 14).

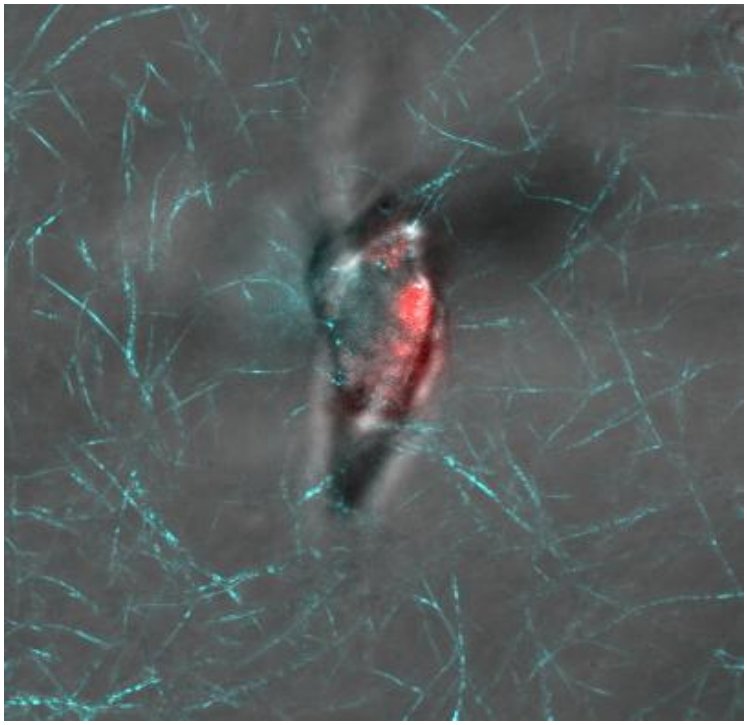

Figure 14: HUVEC (phase contrast) within 3D glycated collagen gel matrix (cyan) infused with EnSens MMP14-activity detection kit reagents (red). Image taken in collaboration with Dr. François Bordeleau.

CHAPTER 4

DISCUSSION

Tumors exhibit many characteristics that distinguish them from surrounding physiological tissue. Here, we focus on two: abnormal vasculature, and extracellular matrix stiffening. In this project, we were interested in investigating and disrupting the relationship between tumor stiffening, angiogenic vascularization, and vascular permeability. Previous work by our lab indicates that collagen cross-linking, which is the primary driving force behind matrix stiffening, is capable of enhancing the angiogenic outgrowth of endothelial cell spheroids.[21,41] In this study, matrix stiffness was controlled via non-enzymatic glycation reactions, which can produce a three-fold increase in matrix stiffness without affecting matrix architecture. This differs from methods that alter matrix density and composition, which drastically influence matrix architecture, porosity, and the number of available integrin binding sites.[38–40] By applying this technique to an existing *ex ovo* angiogenesis model in which constructs composed of collagen gels sandwiched between nylon meshes are grafted to the chorioallantoic membranes of chicken embryos, we observed that cross-linked constructs experience significantly enhanced angiogenic vascularization, as indicated by an increase in vascular density relative to compliant constructs.[83] This finding suggests that tumor matrix stiffening, driven by increased lysyl oxidase expression and secretion, may be partially responsible for the aberration of tumor vasculature.[28]

Matrix metalloproteinases are calcium-dependent enzymes capable of degrading extracellular matrix proteins, enabling cells to migrate through tissues. MT1-MMP, also referred to as MMP-14, is especially relevant to the tumor microenvironment, as it is responsible for cleaving collagen, the increased expression and deposition of which is elevated in cancerous tissue.[19,27,93] Interestingly, MT1-MMP expression is also upregulated in tumor tissues, and our lab has shown that MT1-MMP activity increases with matrix stiffness.[43,82] Furthermore, MT1-MMP has been found to be essential to the ability of endothelial cells to form neovessels.[44]

Based on this information, we were interested in investigating the role of MT1-MMP activity in stiffness-sensitive angiogenic outgrowth. Surprisingly, we found that while inhibiting MMP activity via treatment with GM6001 has no effect on the vascularization of compliant collagen constructs, it eliminates the stimulating effect that cross-linking has on construct vascularization *ex ovo*. Interestingly, active MMP-14 is capable of activating MMP-2 and MMP-9, releasing sequestered growth factors, and even promoting the expression of growth factors, including VEGF.[43,44,94] Therefore, MT1-MMP activity may facilitate and promote angiogenesis in stiff tissues, such as tumors, both directly and indirectly.

With respect to abnormal tumor vasculature, perhaps even more disruptive than excessive branching is the onset of hyperpermeability, which yields vessels that leak fluid, which accumulates within the interstitial space, resulting in uniformly high tumor interstitial pressures that resists flow into the tissue core, diminishes convective extravasation from vasculature within the tumor, and which ultimately leads to hypoxia, acidosis, the rise of aggressive metastatic cells, and resistance to immune cell entry and functionality.[7–14] Previous work by our lab revealed that arterial intima wall stiffening, as observed in arteriosclerosis, promotes endothelial barrier permeability.[45] As the endothelial cell barrier of angiogenic neovessels and tumor microvessels are only surrounded by a thin basement membrane stabilized by pericytes, they are vulnerable to the forces imposed by their surrounding extracellular matrix.[48,49,95] Therefore, we were interested in investigating the effect that matrix stiffening has on vascular permeability. In our pursuit of quantifying the effect that collagen cross-linking has on vascular leakage, we developed a novel *ex ovo* neovessel permeability assay, which was used, in part, to reveal that vasculature grown within stiff tissues are significantly leakier than those grown within compliant ones. This work was carried out alongside an *in vivo* study in which dye extravasation from the tumor vasculature of mice, some treated with β-aminopropionitrile, an inhibitor of collagen cross-linking, revealed that stiffer tumors experience greater vascular leakage.

It has been well established that VE-cadherin phosphorylation is a prime regulator of vascular permeability.[52] In particular, the phosphorylation of residues Y658 and Y685, which are mediated by the phosphorylation of FAK Y397 and Src Y418, leads to the dissociation of p120-catenin and β-catenin from VE-cadherin, which disrupts cytoskeletal attachment and enables VE-cadherin internalization.[51–58] Because recent work by our lab has revealed that matrix stiffening disrupts VE-cadherin localization, we decided to investigate the effect that FAK Y397 phosphorylation inhibition has on stiffness-sensitive vascular permeability.[82] To achieve this, we employed PF573228, an ATP analogue that selectively inhibits FAK Y397 phosphorylation, which is currently undergoing anti-cancer preclinical trials.[59,69,70,96] We began by quantifying the effect that FAK inhibition has on monolayer permeability, and found that while treatment has no effect on monolayers grown on compliant substrates, it significantly reduces the permeability of those grown on stiff ones, with a concentration of 100 nM eliciting the greatest effect.

In lieu of data regarding appropriate dosage values for animal experiments, we applied 1 μM of inhibitor topically to collagen constructs grafted to the chorioallantoic membranes of chicken embryos cultured *ex ovo*, and were surprised to find that treatment with PF573228 normalized the permeability of neovessels within cross-linked constructs without disturbing those within compliant ones. This finding suggests that pre-treating cancer patients with FAK inhibitors might enhance the efficacy of existing systemic chemotherapeutics by normalizing leaky tumor vessels, and thus alleviating fluid accumulation and flow stagnation.

As FAK inhibition alleviated stiffness-induced hyperpermeability, we hypothesized that FAK Y397 phosphorylation would increase with matrix stiffness, which in turn would suggest that VE-cadherin Y658 and or Y685 phosphorylation would increase with matrix stiffness. We were surprised to find that, in our *in vitro* system, collagen cross-linking does not influence FAK activity. For this reason, we decided to investigate Src Y418, as its role as a mediator of vascular permeability is regulated by FAK, and as the disruption of FAK Y397 phosphorylation prevents the formation of FAK-Src complexes.[51,57,70,71,97] Interestingly, we found that increasing

matrix stiffness significantly enhances Src Y418 phosphorylation, and that FAK inhibition has no effect on Src activity. Furthermore, we found that VE-cadherin Y685 phosphorylation increased with matrix stiffness in a manner dependent on FAK Y397 phosphorylation. These findings suggest that Src activity is responsible for stiffness-sensitive vascular permeability in a manner dependent on the phosphorylation of FAK Y397 (Figure 15).

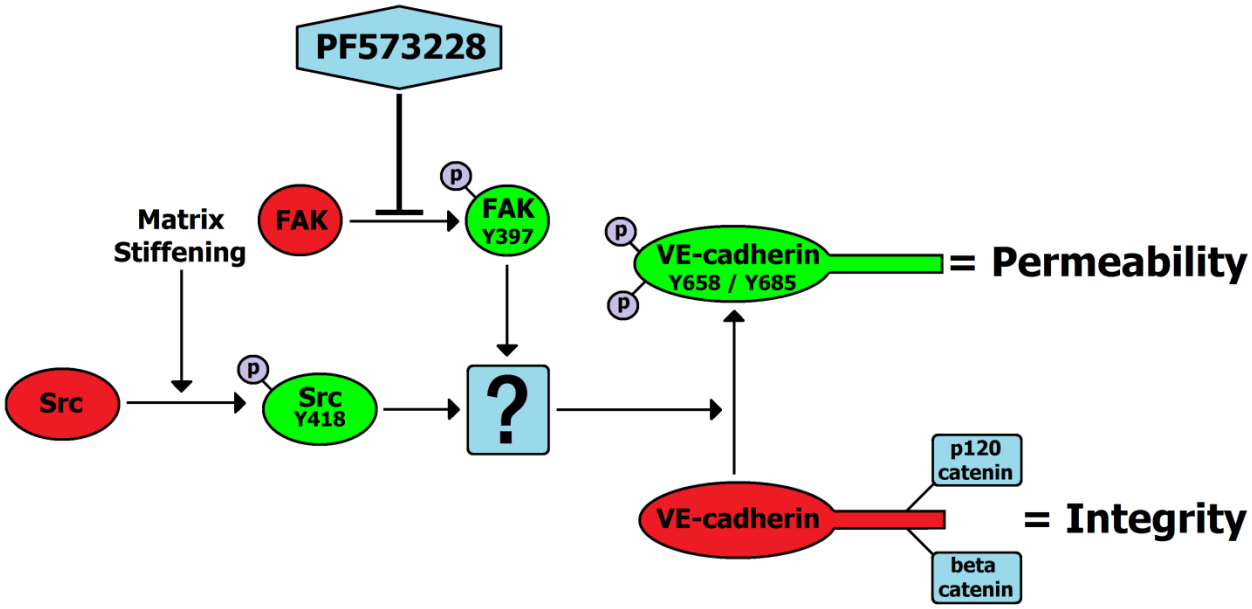

Figure 15: Proposed mechanism to explain stiffness-sensitive permeability in a manner that agrees with the presented data. Matrix stiffening promotes the phosphorylation of Src Y418, which promotes the phosphorylation of VE-cadherin residues Y658 and or Y685 in a way that depends on FAK Y397 phosphorylation. VE-cadherin phosphorylation triggers dissociation of p120-catenin and beta-catenin, which localize and stabilize VE-cadherin at cell-cell junctions. Inhibiting FAK Y397 phosphorylation with PF573228 alleviates stiffness-sensitive permeability.

CHAPTER 5

CONCLUSION

Based on the findings of this project, as well as on the work of a colleague, we believe that the aberration of tumor vasculature characteristics can be alleviated or prevented by inhibiting the formation of collagen cross-links, resulting in tumors that are less aggressive, more receptive to treatment, and more vulnerable to immunological attacks. This can be achieved by administering inhibitors of the lysyl oxidase family, including BAPN, AB0023, and tetrathiomolybdate (TM). BAPN has a history of clinical use outside of cancer therapy, but has been reported to cause osteo- and angio- lathyrism, which are characterized by bone deformity and aortic aneurysms, respectively.[98–100] On the other hand, AB0023, a noncompetitive allosteric inhibitor of lysyl oxidase-like 2 (LOXL2), is a novel antibody that has been found capable of significantly reducing collagen cross-linking within xenograft models; in one study, it was reported to be more effective than BAPN in preventing tissue stiffening.[101] Furthermore, TM, a copper chelator, has already passed through a phase I clinical trial, and is currently undergoing phase II trials.[102–104] By disrupting tumor stiffening, we propose that angiogenic vascularization would not go awry, and that tumor vessels would not become so leaky as to cause fluid accumulation, flow stagnation and reversal, and vessel collapse.

We also believe that existing cancer treatment methods can be enhanced via pre-treatment with inhibitors of focal adhesion kinase tyrosine residue 397, which we have been shown to normalize vascular permeability. As increases in FAK expression and activity have been correlated to tumor progression, and as it has been implicated as critical to cancer cell growth, survival, motility, transformation, and to angiogenesis itself, it has been considered a potential therapeutic target for over a decade.[59,105] Consequently, over a dozen FAK inhibitors many of which disrupt phosphorylation, and some of which disrupt scaffolding functions, have been developed, and are currently undergoing clinical trials.[105] In this work, we presented

evidence indicating that these inhibitors, namely those that target FAK Y397 phosphorylation, and those that disrupt FAK's ability to interact or to form complexes with Src, have greater utility in cancer therapy than previously realized. For example, PF562261, an analogue of PF573228, has already passed a phase I clinical trials, and has even been shown capable of preventing VE-cadherin Y658 phosphorylation, resulting in improved endothelial cell barrier function .[106,57]

To substantiate the results presented here, we propose an investigation into the effects that matrix stiffness and PF573228 have on the phosphorylation of VE-cadherin Y658. This requires access to the proper anti-phospho-VE-cadherin antibody, which has been discontinued. Furthermore, it would be interesting to evaluate the effect that FAK inhibition has VE-cadherin localization within endothelial cells grown on stiff substrates, or on those grown within stiff constructs. Finally, because we found Src to be responsive to changes in matrix stiffness in a FAK-dependent manner, it would be interesting to evaluate the ability of an inhibitor of Src Y418 phosphorylation to alleviate or prevent stiffness-sensitive hyperpermeability. Examples of such inhibitors include PP1, which has been reported to reduce vascular permeability *in vivo*, and AP23846, which is more potent and more selective toward Y418, but is less frequently used.[58,107]

CHAPTER 6

FUTURE DIRECTIONS

In this project, we have shown that vascularization via angiogenesis occurs to a greater extent in stiff tissues relative to compliant ones, and that the vessels grown within stiff tissues are significantly leakier than those formed within compliant ones. Expanding upon this finding, we believe that it would be interesting to investigate the effects that matrix stiffening would have on the characteristics of vasculature established within compliant tissues. As tumors begin as relatively compliant masses of cells that stiffen over time and that must co-opt and engulf existing vasculature to grow beyond a miniscule size, such a study would reveal the changes in the characteristics of the initial vessels.[28,108–110] Perhaps the most direct way to achieve this would be to induce the cross-linking of collagen fibers within compliant constructs post-vascularization, which itself could be achieved by introducing exogenous members of the lysyl oxidase family. For example, in one study, exogenous LOXL2 was used to stiffen collagen-rich implants, and it was found that changes in final tensile values, as well as in stiffening kinetics, could be controlled by adjusting LOXL2 concentration.[111] Alternatively, a collagen gel infused with photo-cross-linkers could be used.[112]

Even more interesting would be an investigation into the reversibility of stiffness-induced vascular characteristics. This study could be conducted via the application cross-link-breakers to our existing glycated collagen construct model, or via the use of a hydrogel system with tunable post-gelation stiffness. Though a literature search failed to identify any lysyl oxidase cross-link-breakers, a number of advanced glycation end product cross-link-breakers do exist, including TRC4186, C36, and ALT-711. TRC4186, an AGE-breaker designed to combat cardiomyopathy and nephropathy in diabetics, has undergone phase I clinical trials, and is currently undergoing phase II trials in India.[113–115] C36, also designed to prevent diabetes-associated cardiovascular problems, has been shown to break AGE-derived collagen cross-links *in vitro* and *in vivo*.[116]

Finally, ALT-711, which passed phase I and II clinical trials under the name Alagebrium, was found capable of significantly lowering the stiffness of left ventricle stiffening within the hearts of patients over a one year study via the elimination of AGE-derived cross-links.[117] Alternative to the glycated collagen construct model used within this project, an alginate-based hydrogel that incorporates reversible cross-links, which is capable of undergoing both stiffening *and* softening as late as two weeks post-gelation in a spatially controlled manner, could be used to evaluate the reversibility of stiffness-induced vascular characteristics.[118] In the context of cancer therapy, if it were to be found that reducing tumor stiffness induces a vascular normalization response, then perhaps the efficacy of existing cancer treatment methods could be enhanced by incorporating pre-treatments that target tumor stiffness.

Separate from cancer research, an investigation into the reversibility of stiffness-sensitive vascular characteristics might also be of interest to engineers who design tissue constructs. We imagine constructs designed with degradable cross-links, which makes them resistant to breaking during implantation, and which promotes angiogenic vascularization and cell migration to facilitate host-construct integration, but eventually soften to physiological levels.

REFERENCES

(1) Siegel, R. L.; Miller, K. D.; Jemal, A. Cancer Statistics, 2016. *CA. Cancer J. Clin.* **2015**, *66* (1).

(2) Mehlen, P.; Puisieux, A. Metastasis: A Question of Life or Death. *Nat. Rev. Cancer* **2006**, *6* (6), 449–458.

(3) Monteiro, J.; Fodde, R. Cancer Stemness and Metastasis: Therapeutic Consequences and Perspectives. *Eur. J. Cancer* **2010**, *46* (7), 1198–1203.

(4) NIH. Cancer Treatment: Types of Treatment http://www.cancer.gov/about-cancer/treatment/types.

(5) Sudhakar, A. History of Cancer, Ancient and Modern Treatment Methods. *J. Cancer Sci. Ther.* **2009**, *1* (2), 1–4.

(6) Rockwell, S.; Dobrucki, I. T.; Kim, E. Y.; Marrison, S. T.; Vu, V. T. Hypoxia and Radiation Therapy: Past History, Ongoing Research, and Future Promise. *Curr. Mol. Med.* **2009**, *9* (4), 442–458.

(7) Jain, R. Barriers to Drug-Delivery in Solid Tumors. *Sci. Am.* **1994**, *271* (1), 58–65.

(8) Goel, S.; Wong, A. H.-K.; Jain, R. K. Vascular Normalization as a Therapeutic Strategy for Malignant and Nonmalignant Disease. *Cold Spring Harb. Perspect. Med.* **2012**, *2* (3), a006486.

(9) Jain, R. Determinants of Tumor Blood-Flow - a Review. *Cancer Res.* **1988**, *48* (10), 2641–2658.

(10) Dudley, A. C. Tumor Endothelial Cells. *Cold Spring Harb. Perspect. Med.* **2012**, *2* (3), a006536.

(11) Jain, R. K. Physiological Resistance to the Treatment of Solid Tumors. In *Drug resistance in oncology*; Marcel Dekker, Inc., 270 Madison Avenue, New York, New York 10016, USA; Marcel Dekker, Inc., Basel, Switzerland, 1993; pp 85–105.

(12) Sevick, E.; Jain, R. Viscous Resistance to Blood-Flow in Solid Tumors - Effect of Hematocrit on Intratumor Blood-Viscosity. *Cancer Res.* **1989**, *49* (13), 3513–3519.

(13) Munn, L. Aberrant Vascular Architecture in Tumors and Its Importance in Drug-Based Therapies. *Drug Discov. Today* **2003**, *8* (9), 396–403.

(14) Jain, R. K. Antiangiogenesis Strategies Revisited: From Starving Tumors to Alleviating Hypoxia. *Cancer Cell* **2014**, *26* (5), 605–622.

(15) Patan, S. Vasculogenesis and Angiogenesis as Mechanisms of Vascular Network Formation, Growth and Remodeling. *J. Neurooncol.* **2000**, *50* (1–2), 1–15.

(16) Folkman, J. Isolation of a Tumor Factor Responsible for Angiogenesis. *J. Exp. Med.* **1971**, *133* (2), 275–288.

(17) Folkman, J.; Bach, M.; Rowe, J.; Davidoff, F.; Lambert, P.; Hirsch, C.; Goldberg, A.; Hiatt, H.; Glass, J.; Henshaw, E. Tumor Angiogenesis - Therapeutic Implications. *N. Engl. J. Med.* **1971**, *285* (21), 1182-.

(18) Webb, T. Vascular Normalization: Study Examines How Antiangiogenesis Therapies Work. *JNCI J. Natl. Cancer Inst.* **2005**, *97* (5), 336–337.

(19) Lu, P.; Weaver, V. M.; Werb, Z. The Extracellular Matrix: A Dynamic Niche in Cancer Progression. *J. Cell Biol.* **2012**, *196* (4), 395–406.

(20) Nagelkerke, A.; Bussink, J.; Rowan, A. E.; Span, P. N. The Mechanical Microenvironment in Cancer: How Physics Affects Tumours. *Semin. Cancer Biol.* **2015**, *35*, 62–70.

(21) Ng, M. R.; Brugge, J. S. A Stiff Blow from the Stroma: Collagen Crosslinking Drives Tumor Progression. *Cancer Cell* **2009**, *16* (6), 455–457.

(22) Avery, N. C.; Bailey, A. J. Enzymic and Non-Enzymic Cross-Linking Mechanisms in Relation to Turnover of Collagen: Relevance to Aging and Exercise. *Scand. J. Med. Sci. Sport.* **2005**, *15* (4), 231–240.

(23) Gkogkolou, P.; Böhm, M. Advanced Glycation End Products: Key Players in Skin Aging? *Dermatoendocrinol.* **2012**, *4* (3), 259–270.

(24) Van Heijst, W. J.; Niessen, H. W.; Hoekman, K.; Schalkwijk, C. G. Advanced Glycation End Products in Human Cancer Tissues. *Ann. N. Y. Acad. Sci.* **2005**, *1043* (1), 725–733.

(25) Smith-Mungo, L. I.; Kagan, H. M. Lysyl Oxidase: Properties, Regulation and Multiple Functions in Biology. *Matrix Biol.* **1998**, *16* (7), 387–398.

(26) Erler, J. T.; Bennewith, K. L.; Nicolau, M.; Dornhöfer, N.; Kong, C.; Le, Q.-T.; Chi, J.-T. A.; Jeffrey, S. S.; Giaccia, A. J. Lysyl Oxidase Is Essential for Hypoxia-Induced Metastasis. *Nature* **2006**, *440* (7088), 1222–1226.

(27) Levental, K. R.; Yu, H.; Kass, L.; Lakins, J. N.; Egeblad, M.; Erler, J. T.; Fong, S. F. T.; Csiszar, K.; Giaccia, A.; Weninger, W.; et al. Matrix Crosslinking Forces Tumor Progression by Enhancing Integrin Signaling. *Cell* **2009**, *139* (5), 891–906.

(28) Butcher, D. T.; Alliston, T.; Weaver, V. M. A Tense Situation: Forcing Tumour Progression. *Nat. Rev. Cancer* **2009**, *9* (2), 108–122.

(29) Chicurel, M. E.; Chen, C. S.; Ingber, D. E. Cellular Control Lies in the Balance of Forces. *Curr. Opin. Cell Biol.* **1998**, *10* (2), 232–239.

(30) Wang, J. H.-C.; Thampatty, B. P. An Introductory Review of Cell Mechanobiology. *Biomech. Model. Mechanobiol.* **2006**, *5* (1), 1–16.

(31) Jansen, K. A.; Donato, D. M.; Balcioglu, H. E.; Schmidt, T.; Danen, E. H. J.; Koenderink, G. H. A Guide to Mechanobiology: Where Biology and Physics Meet. *Biochim. Biophys. Acta - Mol. Cell Res.* **2015**, *1853* (11), 3043–3052.

(32) Bae, Y. H.; Mui, K. L.; Hsu, B. Y.; Liu, S.-L.; Cretu, A.; Razinia, Z.; Xu, T.; Puré, E.; Assoian, R. K. A FAK-Cas-Rac-Lamellipodin Signaling Module Transduces Extracellular Matrix Stiffness into Mechanosensitive Cell Cycling. *Sci. Signal.* **2014**, *7* (330), ra57.

(33) Baker, A.-M.; Bird, D.; Lang, G.; Cox, T. R.; Erler, J. T. Lysyl Oxidase Enzymatic Function Increases Stiffness to Drive Colorectal Cancer Progression through FAK. *Oncogene* **2013**, *32* (14), 1863–1868.

(34) Mittal, K.; Ebos, J.; Rini, B. Angiogenesis and the Tumor Microenvironment: Vascular Endothelial Growth Factor and Beyond. *Semin. Oncol.* **2014**, *41* (2), 235–251.

(35) Jain, R. K. Normalizing Tumor Vasculature with Anti-Angiogenic Therapy: A New Paradigm for Combination Therapy. *Nat. Med.* **2001**, *7* (9), 987–989.

(36) Tranqui, L.; Tracqui, P. Mechanical Signalling and Angiogenesis. The Integration of Cell–extracellular Matrix Couplings. *Comptes Rendus l'Académie des Sci. - Ser. III - Sci. la Vie* **2000**, *323* (1), 31–47.

(37) Presta, M.; Dell'Era, P.; Mitola, S.; Moroni, E.; Ronca, R.; Rusnati, M. Fibroblast Growth Factor/fibroblast Growth Factor Receptor System in Angiogenesis. *Cytokine Growth Factor Rev.* **2005**, *16* (2), 159–178.

(38) Cross, V. L.; Zheng, Y.; Won Choi, N.; Verbridge, S. S.; Sutermaster, B. A.; Bonassar, L. J.; Fischbach, C.; Stroock, A. D. Dense Type I Collagen Matrices That Support Cellular Remodeling and Microfabrication for Studies of Tumor Angiogenesis and Vasculogenesis in Vitro. *Biomaterials* **2010**, *31* (33), 8596–8607.

(39) Edgar, L. T.; Underwood, C. J.; Guilkey, J. E.; Hoying, J. B.; Weiss, J. A. Extracellular Matrix Density Regulates the Rate of Neovessel Growth and Branching in Sprouting Angiogenesis. *PLoS One* **2014**, *9* (1), e85178.

(40) Rao, R. R.; Peterson, A. W.; Ceccarelli, J.; Putnam, A. J.; Stegemann, J. P. Matrix Composition Regulates Three-Dimensional Network Formation by Endothelial Cells and Mesenchymal Stem Cells in Collagen/fibrin Materials. *Angiogenesis* **2012**, *15* (2), 253–264.

(41) Mason, B. N.; Starchenko, A.; Williams, R. M.; Bonassar, L. J.; Reinhart-King, C. A. Tuning Three-Dimensional Collagen Matrix Stiffness Independently of Collagen Concentration Modulates Endothelial Cell Behavior. *Acta Biomater.* **2013**, *9* (1), 4635–4644.

(42) Haage, A.; Schneider, I. C. Cellular Contractility and Extracellular Matrix Stiffness Regulate Matrix Metalloproteinase Activity in Pancreatic Cancer Cells. *FASEB J.* **2014**, *28* (8), 3589–3599.

(43) Haage, A.; Nam, D. H.; Ge, X.; Schneider, I. C. Matrix Metalloproteinase-14 Is a Mechanically Regulated Activator of Secreted MMPs and Invasion. *Biochem. Biophys. Res. Commun.* **2014**, *450* (1), 213–218.

(44) Chun, T.-H.; Sabeh, F.; Ota, I.; Murphy, H.; McDonagh, K. T.; Holmbeck, K.; Birkedal-Hansen, H.; Allen, E. D.; Weiss, S. J. MT1-MMP–dependent Neovessel Formation within the Confines of the Three-Dimensional Extracellular Matrix. *J. Cell Biol.* **2004**, *167* (4), 757–767.

(45) Huynh, J.; Nishimura, N.; Rana, K.; Peloquin, J. M.; Califano, J. P.; Montague, C. R.; King, M. R.; Schaffer, C. B.; Reinhart-King, C. a. Age-Related Intimal Stiffening Enhances Endothelial Permeability and Leukocyte Transmigration. *Sci. Transl. Med.* **2011**, *3* (112), 112ra122-112ra122.

(46) Allaire, E.; Clowes, A. W. The Intimal Hyperplastic Response. *Ann. Thorac. Surg.* **1997**, *64* (4), S38–S46.

(47) Snow, A. D.; Bolender, R. P.; Wight, T. N.; Clowes, A. W. Heparin Modulates the Composition of the Extracellular Matrix Domain Surrounding Arterial Smooth Muscle Cells. *Am. J. Pathol.* **1990**, *137* (2), 313–330.

(48) Vontell, D.; Armulik, A.; Betsholtz, C. Pericytes and Vascular Stability. *Exp. Cell Res.* **2006**, *312* (5), 623–629.

(49) Califano, J. P.; Reinhart-King, C. A. Exogenous and Endogenous Force Regulation of Endothelial Cell Behavior. *J. Biomech.* **2010**, *43* (1), 79–86.

(50) Dejana, E.; Vestweber, D. The Role of VE-Cadherin in Vascular Morphogenesis and Permeability Control. *Prog. Mol. Biol. Transl. Sci.* **2013**, *116*, 119–144.

(51) Sarelius, I. H.; Glading, A. J. Control of Vascular Permeability by Adhesion Molecules. *Tissue barriers* **2015**, *3* (1–2), e985954.

(52) Sidibe, A.; Imhof, B. A. VE-Cadherin Phosphorylation Decides: Vascular Permeability or Diapedesis. *Nat. Immunol.* **2014**, *15* (3), 215–217.

(53) Hatanaka, K.; Simons, M.; Murakami, M. Phosphorylation of VE-Cadherin Controls Endothelial Phenotypes via p120-Catenin Coupling and Rac1 Activation. *Am. J. Physiol. - Hear. Circ. Physiol.* **2011**, *300* (1).

(54) Gavard, J. Endothelial Permeability and VE-Cadherin. *Cell Adh. Migr.* **2013**, *7* (6), 465–471.

(55) Giannotta, M.; Trani, M.; Dejana, E. VE-Cadherin and Endothelial Adherens Junctions: Active Guardians of Vascular Integrity. *Dev. Cell* **2013**, *26* (5), 441–454.

(56) Sidibe, A.; Polena, H.; Razanajatovo, J.; Mannic, T.; Chaumontel, N.; Bama, S.; Marechal, I.; Huber, P.; Gulino-Debrac, D.; Bouillet, L.; et al. Dynamic Phosphorylation of VE-Cadherin Y685 throughout Mouse Estrous Cycle in Ovary and Uterus. *AJP Hear. Circ. Physiol.* **2014**, *307* (3), H448–H454.

(57) Jean, C.; Chen, X. L.; Nam, J.-O.; Tancioni, I.; Uryu, S.; Lawson, C.; Ward, K. K.; Walsh, C. T.; Miller, N. L. G.; Ghassemian, M.; et al. Inhibition of Endothelial FAK Activity Prevents Tumor Metastasis by Enhancing Barrier Function. *J. Cell Biol.* **2014**, *204* (2), 247–263.

(58) He, Y.-X.; Liu, J.; Guo, B.; Wang, Y.-X.; Pan, X.; Li, D.; Tang, T.; Chen, Y.; Peng, S.; Bian, Z.; et al. Src Inhibitor Reduces Permeability without Disturbing Vascularization and Prevents Bone Destruction in Steroid-Associated Osteonecrotic Lesions in Rabbits. *Sci. Rep.* **2015**, *5*, 8856.

(59) Sulzmaier, F. J.; Jean, C.; Schlaepfer, D. D. FAK in Cancer: Mechanistic Findings and Clinical Applications. *Nat. Rev. Cancer* **2014**, *14* (9), 598–610.

(60) Wheeler, D. L.; Iida, M.; Dunn, E. F. The Role of Src in Solid Tumors. *Oncologist* **2009**, *14* (7), 667–678.

(61) Thomas, S. M.; Brugge, J. S. Cellular Functions Regulated by Src Family Kinases. *Annu. Rev. Cell Dev. Biol.* **1997**, *13* (1), 513–609.

(62) Zebda, N.; Dubrovskyi, O.; Birukov, K. G. Focal Adhesion Kinase Regulation of Mechanotransduction and Its Impact on Endothelial Cell Functions. *Microvasc. Res.* **2012**, *83* (1), 71–81.

(63) Wu, M. H.; Guo, M.; Yuan, S. Y.; Granger, H. J. Focal Adhesion Kinase Mediates Porcine Venular Hyperpermeability Elicited by Vascular Endothelial Growth Factor. *J. Physiol.* **2003**, *552* (Pt 3), 691–699.

(64) Usatyuk, P. V. Regulation of Reactive Oxygen Species-Induced Endothelial Cell-Cell and Cell-Matrix Contacts by Focal Adhesion Kinase and Adherens Junction Proteins. *AJP Lung Cell. Mol. Physiol.* **2005**, *289* (6), L999–L1010.

(65) Kim, M. P.; Park, S. I.; Kopetz, S.; Gallick, G. E. Src Family Kinases as Mediators of Endothelial Permeability: Effects on Inflammation and Metastasis. *Cell Tissue Res.* **2009**, *335* (1), 249–259.

(66) Chen, X. L.; Nam, J.-O.; Jean, C.; Lawson, C.; Walsh, C. T.; Goka, E.; Lim, S.-T.; Tomar, A.; Tancioni, I.; Uryu, S.; et al. VEGF-Induced Vascular Permeability Is Mediated by FAK. *Dev. Cell* **2012**, *22* (1), 146–157.

(67) Belvitch, P.; Dudek, S. M. Role of FAK in S1P-Regulated Endothelial Permeability. *Microvasc. Res.* **2012**, *83* (1), 22–30.

(68) Seong, J.; Tajik, A.; Sun, J.; Guan, J.-L.; Humphries, M. J.; Craig, S. E.; Shekaran, A.; Garcia, A. J.; Lu, S.; Lin, M. Z.; et al. Distinct Biophysical Mechanisms of Focal Adhesion Kinase Mechanoactivation by Different Extracellular Matrix Proteins. *Proc. Natl. Acad. Sci.* **2013**, *110* (48), 19372–19377.

(69) Slack-Davis, J. K.; Martin, K. H.; Tilghman, R. W.; Iwanicki, M.; Ung, E. J.; Autry, C.; Luzzio, M. J.; Cooper, B.; Kath, J. C.; Roberts, W. G.; et al. Cellular Characterization of a Novel Focal Adhesion Kinase Inhibitor. *J. Biol. Chem.* **2007**, *282* (20), 14845–14852.

(70) Yoon, H.; Dehart, J. P.; Murphy, J. M.; Lim, S.-T. S. Understanding the Roles of FAK in Cancer: Inhibitors, Genetic Models, and New Insights. *J. Histochem. Cytochem.* **2015**, *63* (2), 114–128.

(71) Bolós, V.; Gasent, J. M.; López-Tarruella, S.; Grande, E. The Dual Kinase Complex FAK-Src as a Promising Therapeutic Target in Cancer. *Onco. Targets. Ther.* **2010**, *3*, 83–97.

(72) Mason, B. N.; Reinhart-King, C. A. Controlling the Mechanical Properties of Three-Dimensional Matrices via Non-Enzymatic Collagen Glycation. *Organogenesis* **2013**, *9* (2), 70–75.

(73) Zijlstra, A.; Seandel, M.; Kupriyanova, T. A.; Partridge, J. J.; Madsen, M. A.; Hahn-Dantona, E. A.; Quigley, J. P.; Deryugina, E. I. Proangiogenic Role of Neutrophil-like Inflammatory Heterophils during Neovascularization Induced by Growth Factors and Human Tumor Cells. *Blood* **2006**, *107* (1), 317–327.

(74) Dvorak, H.; Brown, L.; Detmar, M.; Dvorak, A. Vascular Permeability Factor/vascular Endothelial Growth Factor, Microvascular Hyperpermeability, and Angiogenesis. *Am. J. Pathol.* **1995**, *146* (5), 1029–1039.

(75) Califano, J. P.; Reinhart-King, C. A. A Balance of Substrate Mechanics and Matrix Chemistry Regulates Endothelial Cell Network Assembly. *Cell. Mol. Bioeng.* **2008**, *1* (2–3), 122–132.

(76) Wang, Y.-L.; Pelham, R. J. Preparation of a Flexible, Porous Polyacrylamide Substrate for Mechanical Studies of Cultured Cells; 1998; pp 489–496.

(77) Mini-PROTEAN ® Tetra Cell Instruction Manual http://www.bio-rad.com/webroot/web/pdf/lsr/literature/10007296D.pdf.

(78) Mini Trans-Blot ® Electrophoretic Transfer Cell Instruction Manual http://www.bio-rad.com/webroot/web/pdf/lsr/literature/M1703930.pdf.

(79) SuperSignal West Pico Chemiluminescent Substrate https://tools.thermofisher.com/content/sfs/manuals/MAN0011303_SupSig_West_Pico_Chemilum_Subs_UG.pdf.

(80) SuperSignal West Dura Extended Duration Substrate https://tools.thermofisher.com/content/sfs/manuals/MAN0011307_SupSig_West_Dura_Extend_Dur_Subs_UG.pdf.

(81) SuperSignal West Femto Maximum Sensitivity Substrate https://tools.thermofisher.com/content/sfs/manuals/MAN0011345_SupSig_West_Femto_MaxSensi_Subs_UG.pdf.

(82) Mason, B. N.; Bordeleau, F.; Lollis, E. M.; Mazzola, M. C.; Zanotelli, M. R.; Somasegar, S.; Califano, J. P.; Montague, C. R.; LaValley, D.; Huynh, J.; et al. Matrix Stiffening Promotes a Tumor Vasculature Phenotype. *Proc. Natl. Acad. Sci.* **(in press)**.

(83) Nguyen, M.; Shing, Y.; Folkman, J. Quantitation of Angiogenesis and Antiangiogenesis in the Chick Embryo Chorioallantoic Membrane. *Microvasc. Res.* **1994**, *47* (1), 31–40.

(84) Pink, D. B. S.; Schulte, W.; Parseghian, M. H.; Zijlstra, A.; Lewis, J. D. Real-Time Visualization and Quantitation of Vascular Permeability in Vivo: Implications for Drug Delivery. *PLoS One* **2012**, *7* (3), 1–10.

(85) Grobelny, D.; Poncz, L.; Galardy, R. E. Inhibition of Human Skin Fibroblast Collagenase, Thermolysin, and Pseudomonas Aeruginosa Elastase by Peptide Hydroxamic Acids. *Biochemistry* **1992**, *31* (31), 7152–7154.

(86) Barnes, A. E.; Jensen, W. N. Blood Volume and Red Cell Concentration in the Normal Chick Embryo. *Am. J. Physiol.* **1959**, *197* (2), 403–405.

(87) Gavard, J.; Gutkind, J. S. VEGF Controls Endothelial-Cell Permeability by Promoting the Beta-Arrestin-Dependent Endocytosis of VE-Cadherin. *Nat. Cell Biol.* **2006**, *8* (11), 1223–1234.

(88) Zan, L.; Zhang, X.; Xi, Y.; Wu, H.; Song, Y.; Teng, G.; Li, H.; Qi, J.; Wang, J. Src Regulates Angiogenic Factors and Vascular Permeability after Focal Cerebral Ischemia-Reperfusion. *Neuroscience* **2014**, *262*, 118–128.

(89) Sampath Narayanan, A.; Siegel, R. C.; Martin, G. R. On the Inhibition of Lysyl Oxidase by β-Aminopropionitrile. *Biochem. Biophys. Res. Commun.* **1972**, *46* (2), 745–751.

(90) Schütze, F.; Röhrig, F.; Vorlová, S.; Gätzner, S.; Kuhn, A.; Ergün, S.; Henke, E. Inhibition of Lysyl Oxidases Improves Drug Diffusion and Increases Efficacy of Cytotoxic Treatment in 3D Tumor Models. *Sci. Rep.* **2015**, *5*, 17576.

(91) How EnSens® Technology Works https://www.biomol.de/dateien/Enzium--MMP-Selectivity.pdf.

(92) EnSens® Fluorescent 3D Live Cell Imaging Kit for MMP-14 Activity Tracking http://enziumlabs.com/image/data/MMP14 3D Cell Imaging Kit.pdf.

(93) Provenzano, P. P.; Inman, D. R.; Eliceiri, K. W.; Knittel, J. G.; Yan, L.; Rueden, C. T.; White, J. G.; Keely, P. J.; McCormack, V.; Silva, I. dos S.; et al. Collagen Density Promotes Mammary Tumor Initiation and Progression. *BMC Med.* **2008**, *6* (1), 11.

(94) Sounni, N. E.; Devy, L.; Hajitou, A.; Frankenne, F.; Munaut, C.; Gilles, C.; Deroanne, C.; Thompson, E. W.; Foidart, J. M.; Noel, A. MT1-MMP Expression Promotes Tumor Growth and Angiogenesis through an up-Regulation of Vascular Endothelial Growth Factor Expression. *FASEB J.* **2002**, *16* (6), 555–564.

(95) Davis, G. E. Endothelial Extracellular Matrix: Biosynthesis, Remodeling, and Functions During Vascular Morphogenesis and Neovessel Stabilization. *Circ. Res.* **2005**, *97* (11), 1093–1107.

(96) Infusino, G. A.; Jacobson, J. R. Endothelial FAK as a Therapeutic Target in Disease. *Microvasc. Res.* **2012**, *83* (1), 89–96.

(97) Tai, Y.-L.; Chen, L.-C.; Shen, T.-L. Emerging Roles of Focal Adhesion Kinase in Cancer. *Biomed Res. Int.* **2015**, *2015*, 690690.

(98) Miana, M.; Galán, M.; Martínez-Martínez, E.; Varona, S.; Jurado-López, R.; Bausa-Miranda, B.; Antequera, A.; Luaces, M.; Martínez-González, J.; Rodríguez, C.; et al. The Lysyl Oxidase Inhibitor β-Aminopropionitrile Reduces Body Weight Gain and Improves the Metabolic Profile in Diet-Induced Obesity in Rats. *Dis. Model. Mech.* **2015**, *8* (6).

(99) Peacock, E. E.; Madden, J. W. Administration of Beta-Aminopropionitrile to Human Beings with Urethral Strictures: A Preliminary Report. *Am. J. Surg.* **1978**, *136* (5), 600–605.

(100) Dasler, W.; Milliser, R. V. Experimental Lathyrism in Mice Fed Diets Containing Sweet Peas or Beta-Aminopropionitrile. *Proc. Soc. Exp. Biol. Med.* **1957**, *96* (1), 171–174.

(101) Barry-Hamilton, V.; Spangler, R.; Marshall, D.; McCauley, S.; Rodriguez, H. M.; Oyasu, M.; Mikels, A.; Vaysberg, M.; Ghermazien, H.; Wai, C.; et al. Allosteric Inhibition of Lysyl Oxidase–like-2 Impedes the Development of a Pathologic Microenvironment. *Nat. Med.* **2010**, *16* (9), 1009–1017.

(102) Brewer, G. J.; Dick, R. D.; Grover, D. K.; LeClaire, V.; Tseng, M.; Wicha, M.; Pienta, K.; Redman, B. G.; Jahan, T.; Sondak, V. K.; et al. Treatment of Metastatic Cancer with Tetrathiomolybdate, an Anticopper, Antiangiogenic Agent: Phase I Study. *Clin. Cancer Res.* **2000**, *6* (1).

(103) Phase II Study of Tetrathiomolybdate (TM) in Patients With Breast Cancer https://clinicaltrials.gov/ct2/show/NCT00195091.

(104) Nishioka, T.; Eustace, A.; West, C. Lysyl Oxidase: From Basic Science to Future Cancer Treatment. *Cell Struct. Funct.* **2012**, *37* (1), 75–80.

(105) Golubovskaya, V. Targeting FAK in Human Cancer: From Finding to First Clinical Trials. *Front. Biosci.* **2014**, *19* (4), 687.

(106) Study Of PF-00562271, Including Patients With Pancreatic, Head And Neck, Prostatic Neoplasms https://clinicaltrials.gov/ct2/show/NCT00666926?term=PF00562271&rank=1.

(107) Summy, J. M.; Trevino, J. G.; Lesslie, D. P.; Baker, C. H.; Shakespeare, W. C.; Wang, Y.; Sundaramoorthi, R.; Metcalf, C. A.; Keats, J. A.; Sawyer, T. K.; et al. AP23846, a Novel and Highly Potent Src Family Kinase Inhibitor, Reduces Vascular Endothelial Growth Factor and Interleukin-8 Expression in Human Solid Tumor Cell Lines and Abrogates Downstream Angiogenic Processes. *Mol. Cancer Ther.* **2005**, *4* (12).

(108) Lopez, J. I.; Kang, I.; You, W.-K.; McDonald, D. M.; Weaver, V. M. In Situ Force Mapping of Mammary Gland Transformation. *Integr. Biol.* **2011**, *3* (9), 910.

(109) Folkman, J. Anti-Angiogenesis. *Ann. Surg.* **1972**, *175* (3), 409–416.

(110) Goel, S.; Duda, D. G.; Xu, L.; Munn, L. L.; Boucher, Y.; Fukumura, D.; Jain, R. K. Normalization of the Vasculature for Treatment of Cancer and Other Diseases. *Physiol. Rev.* **2011**, *91* (3), 1071–1121.

(111) Makris, E. A.; Responte, D. J.; Paschos, N. K.; Hu, J. C.; Athanasiou, K. A. Developing Functional Musculoskeletal Tissues through Hypoxia and Lysyl Oxidase-Induced Collagen Cross-Linking. *Proc. Natl. Acad. Sci. U. S. A.* **2014**, *111* (45), E4832-41.

(112) Brinkman, W. T.; Nagapudi, K.; Thomas, B. S.; Chaikof, E. L. Photo-Cross-Linking of Type I Collagen Gels in the Presence of Smooth Muscle Cells: Mechanical Properties, Cell Viability, and Function. *Biomacromolecules* **2003**, *4* (4), 890–895.

(113) Joshi, D.; Gupta, R.; Dubey, A.; Shiwalkar, A.; Pathak, P.; Gupta, R. C.; Chauthaiwale, V.; Dutt, C. TRC4186, a Novel AGE-Breaker, Improves Diabetic Cardiomyopathy and Nephropathy in Ob-ZSF1 Model of Type 2 Diabetes. *J. Cardiovasc. Pharmacol.* **2009**, *54* (1), 72–81.

(114) Chandra, K. P.; Shiwalkar, A.; Kotecha, J.; Thakkar, P.; Srivastava, A.; Chauthaiwale, V.; Sharma, S. K.; Cross, M. R.; Dutt, C. Phase I Clinical Studies of the Advanced Glycation End-Product (AGE)-Breaker TRC4186. *Clin. Drug Investig.* **2009**, *29* (9), 559–575.

(115) CTRI/2009/091/000043 http://www.ctri.nic.in/Clinicaltrials/pmaindet2.php?trialid=319.

(116) Cheng, G.; Wang, L.-L.; Long, L.; Liu, H.-Y.; Cui, H.; Qu, W.-S.; Li, S. Beneficial Effects of C36, a Novel Breaker of Advanced Glycation Endproducts Cross-Links, on the Cardiovascular System of Diabetic Rats. *Br. J. Pharmacol.* **2007**, *152* (8), 1196–1206.

(117) Fujimoto, N.; Hastings, J. L.; Carrick-Ranson, G.; Shafer, K. M.; Shibata, S.; Bhella, P. S.; Abdullah, S. M.; Barkley, K. W.; Adams-Huet, B.; Boyd, K. N.; et al. Cardiovascular Effects of 1 Year of Alagebrium and Endurance Exercise Training in Healthy Older Individuals. *Circ. Hear. Fail.* **2013**, *6* (6), 1155–1164.

(118) Stowers, R. S.; Allen, S. C.; Suggs, L. J. Dynamic Phototuning of 3D Hydrogel Stiffness. *Proc. Natl. Acad. Sci.* **2015**, *112* (7), 1953–1958.

APPENDIX

A.1 Protocol - Western Blot Sample Preparation

Mortar and Pestle Preparation - Per endothelial cell infused glycated collagen gel to be processed, prepare one mortar and one pestle at least one day prior to sample preparation.

1. Wash using Alconox, then rinse using MQ water
2. Submerging in 70% EtOH for 15 minutes, then air dry overnight
3. Wrap in clean aluminum foil, then autoclave (gravity, 15 minutes)
4. Place in a sealable plastic bag, then chill overnight at -80^{o}C

Station Preparation - Perform this step immediately prior to sample preparation in a fume hood

1. Line flat foam trays with paper towels
2. Place 6x Laemmli buffer on ice, as well as labeled tubes
3. Fill bucket with 10 scoops of liquid N_2 using forceps and a cup
4. Transfer chilled mortars and pestles from -80^{o}C to lined foam trays
5. Fill and refill mortars (with pestles inside) with liquid N_2 until evaporation slows

Protein Extraction - Begin performing this step while mortars are filled with liquid N_2

1. Transfer samples from -80^{o}C to liquid N_2, then from liquid N_2 to filled mortars
2. Immediately following N_2 evaporation, crush sample via a few blows with pestle
3. Add 150 µL 6x Laemmli buffer (per 300 µL gel) to crushed sample, then grind to a powder
4. As powder begins to melt, stop grinding (can still mash it, but avoid bubble formation)
5. Once powder is fully liquefied, pour into labeled tubes, flash freeze, and store at -80^{o}C

A.2 Protocol - Chicken Embryo Culture

Egg Procurement - Account for chicken embryo death when planning experiments (unfertilized eggs, dead on arrival, yolk sac rupture during egg cracking, late-stage death, contamination, ...)

1. Order fertilized White Leghorn chicken eggs designated for research purposes
   At Cornell University, eggs can be ordered via phone at (607) 272 - 8970
2. Receive eggs at ≤19°C, and store in a cooler maintained at 12.8°C for ≤7 days
   Alternatively, begin at step *ED0* upon egg delivery

Egg Incubator Preparation - Incubators should be cleaned often to avoid contamination

1. Set the GQF 1500 Professional rocking egg incubator to 37.8°C, and fill the water bath

Chick Incubator Preparation - Incubators should be cleaned often to avoid contamination

1. Obtain a Hova-Bator Circulated Air Incubator, which should consist of a two-unit foam enclosure, a plastic liquid trap, a wire mesh, a heating unit, and a thermometer
2. Wash all incubator components using Alconox and water to remove culture residue
3. Sterilize all incubator components using bleach, followed by a rinse with MQ water
4. Spray all incubator components with 70% EtOH, then air dry overnight
5. Adjust heating unit to achieve 37.8°C, add cups of water to achieve 60% relative humidity

Autoclaved Eggshell Powder Preparation

1. Rinse uncrushed eggshells using water, then soak in Alconox for a few minutes to detach inner-shell membranes, then rinse away membranes and Alconox with warm water
2. Spray eggshells with 70% EtOH, then air-dry overnight in a chemical fume hood
3. Grind dry eggshells into a powder using a mortar and pestle, then transfer into a glass beaker
4. Cover beaker with aluminum foil, then autoclave (30 minutes gravity sterilize)
5. Transfer autoclaved eggshells into labeled 50 mL tubes in a sterile laminar flow hood
6. Store autoclaved eggshells at -20°C until time of use

ED0, Beginning of Culture

1. Press the "Tuner Automatic" button on the GQF 1500 Professional to disable the rocking mechanism, then press and hold the "Tuner Manual" button until the platforms are horizontal
2. Using a dry cloth, gently scrub residue away from eggs (do not use EtOH)
3. Place clean eggs in the rocking egg incubator, then press the "Tuner Automatic" button twice to re-enable the rocking mechanism

ED3, Cracking eggs - Prepare *ex ovo* culture platforms in batches of 10 to 20 to save time
If necessary, save eggshells in a 1000 mL beaker for future use (avoid crushing them)

1. Place a prepared chick incubator nearby the laminar flow cabinet
2. Sterilize the following items, and place them within a sterile laminar flow cabinet
    a) Absorbent pads (lay them out to form a work surface)
    b) Unopened packaged of Fineline Savvi Serve 405 5 oz. plastic tumblers
    c) 1000 mL beaker filled with warm water
    d) AEP 30510400 Zipsafe Sealwrap
    e) Container for spent egg innards
    f) Rubber bands
    g) Kimwipes
    h) Egg carton
    i) Hacksaw and c-clamp
    j) Autoclaved eggshell powder
    k) Plastic Petri dishes
1. Add warm water to each cup (≈ 1/3 full, or ≈ 55 mL per cup)
2. Drape a sheet of plastic wrap over each partially filled cup (leave more than enough slack to form a hammock that rests upon the surface of the water, press the seal wrap against the cup walls (it will stick to the cup), then secure the hammock in place using a rubber band)
3. Spray hammocks with 70% EtOH, wipe using a Kimwipe soaked in 70% EtOH, then air dry
4. Retrieve four eggs from the rocking incubator, spray them using 70% EtOH, place in carton horizontally, and incubate for two minutes (embryos will migrate toward the top of the egg)
5. Preserving the egg's orientation, place it in the c-clamp (contact sides), form a crack along the bottom of the shell via a single tap of the hacksaw (albumin should begin to leak), pry it open, then gently drop egg contents into the hammock of a culture platform (Figure A.1)
6. Immediately deposit a small amount of autoclaved eggshell powder to the albumin at the periphery of the hammock, cap the culture platform with a Petri dish, then place it in a chick incubator (if yolk sac is visibly ripped open, or if egg was unfertilized, or if embryo does not possess a heartbeat, then discard the egg contents and the hammock - cup can be reused)

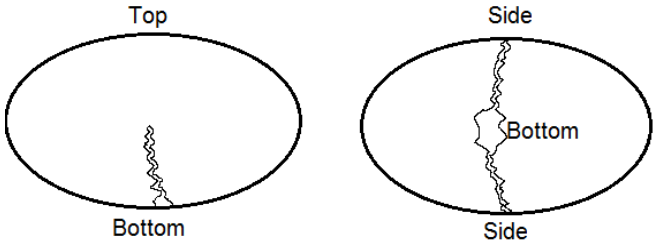

Figure A.1: The ideal crack forms along the lower half of the eggshell's circumference. A slightly larger perforation should be formed at the very bottom to enable the operator to pry the shell open.

ED10, Grafting Constructs

1. Place a chick-containing incubator by the laminar flow cabinet
2. Sterilize the following items, and place them within a sterile laminar flow cabinet
    a. Aluminum foil (lay it out to form a work surface)
    b. 15 mL tube containing 70% EtOH
    c. Sealed dish containing constructs
    d. Metal tweezers
    e. Marker
3. Transfer a chick-containing *ex ovo* culture platform to the laminar flow cabinet
4. Label the *ex ovo* culture platform using a permanent marker (Figure A.2)
5. Use the metal tweezers to place each construct on a predefined section of the chorioallantoic membrane (poking or ripping the CAM will trigger an inflammatory response, so be gentle)
6. Immediately transfer the chick back to the culture incubator
7. Submerge the metal tweezers in 70% EtOH between chicks

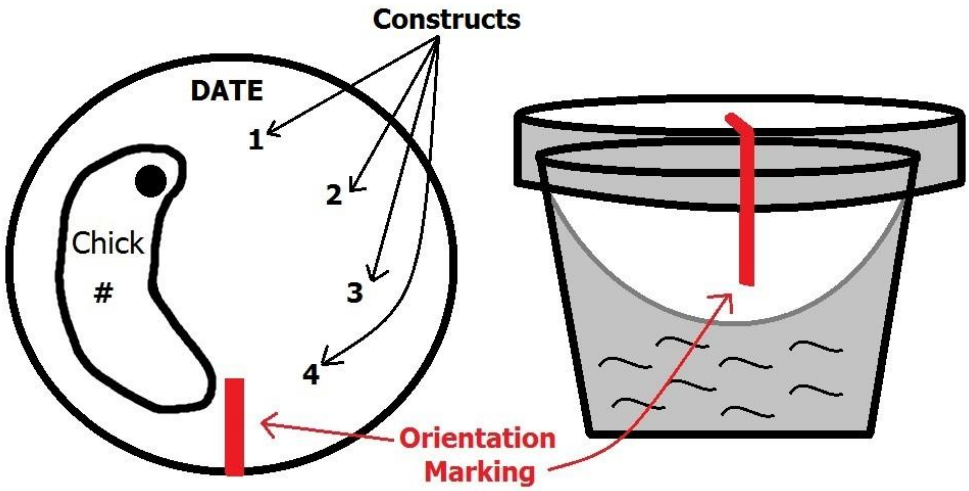

Figure A.2: Grafting positions (place constructs away from the chick, away from major blood vessels, and away from the edge of the hammock), orientation marking (extend from Petri dish to cup), and labels to include.

≤ ED15, End of Culture

Chicken embryos younger than 10.5 days can be disposed of via suffocation (coating the chorioallantoic membrane with oil) or freezing, whereas those older than 10.5 days must be decapitated via a single cut with a sharp pair of scissors prior to disposal